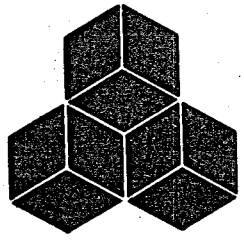

SYSTEMS, SCIENCE AND SOFTWARE

SSS-R-75-2733

GEOHYDROLOGICAL ENVIRONMENTAL EFFECTS OF GEOTHERMAL POWER PRODUCTION PHASE I

BY
J. W. PRITCHETT
S. K. GARG
D. H. BROWNELL, JR.
H. B. LEVINE

FINAL REPORT FOR PHASE I

RESEARCH SPONSORED BY
NATIONAL SCIENCE FOUNDATION
(RESEARCH APPLIED TO NATIONAL NEEDS)
GRANT NO. GI-43885

SEPTEMBER 1975

P.O. BOX 1620, LA JOLLA, CALIFORNIA 92038 TELEPHONE (714) 453-0060

DISCLAIMER

FOREWORD

This final technical report entitled, "Geohydrological Environmental Effects of Geothermal Power Production - Phase I," is submitted by Systems, Science and Software (S^3) to the National Science Foundation (NSF). The report presents the results of the first phase of a three-phase research effort to develop reliable computer simulators whereby field information for a specific geothermal system can be used to predict subsurface environmental effects due to production and reinjection of geothermal fluids. This work, in support of the NSF/RANN Geothermal Research Program, was accomplished under Grant No. GI-43885. Mr. Ritchie Coryell was the NSF Program Manager during the early part of this work; Dr. Ralph N. Perhac was the NSF Program Manager during the latter part of the work.

Mr. John W. Pritchett was the S^3 Principal Investigator for this study. The technical results presented in this report represent the work of a number of S^3 staff members in addition to the authors. It is appropriate to list here the contributors to Sections II through V:

Section II :	S. K. Garg, J. W. Pritchett, M. H. Rice
Section III:	J. W. Pritchett, D. H. Brownell, Jr.
Section IV :	S. K. Garg, J. W. Pritchett, D. H. Brownell, Jr., F. Jones, J. Sweet
Section V :	S. K. Garg, H. B. Levine, A. Nur

Dr. Amos Nur of Stanford University contributed to the preliminary seismic risk analysis; Dr. Harold Helgeson of the University of California at Berkeley served as consultant on the use of his geochemistry code.

A review of the research project was held on July 17, 1975. The work accomplished during Phase I of the project (NSF/RANN Grant GI-43885) was presented in detail and the planned work during Phase II of the project (NSF/RANN Grant

AER 75-14492) was outlined. The participants included all three members of the NSF approved Project Review panel: Mr. Tom Hinrichs (Magma Power Company), Dr. Roy M. Knapp (Department of Petroleum Engineering, University of Texas at Austin) and Dr. Mahinder S. Gulati (Union Oil Company of California, Union Research Center). Mr. Kenneth Brunot of NSF, Western Projects Office, also participated in the review along with Dr. William Brigham of Stanford University and Mr. James M. Nugent of the San Diego Gas & Electric Company. S^3 participants included Drs. Sabodh K. Garg, Donald R. Grine, Howard B. Levine, T. David Riney, Joel Sweet and the Principal Investigator, John W. Pritchett. A document which included copies of all the viewgraphs used during the review presentation was sent to the NSF Program Manager.

Two papers have been published in the technical literature during the course of the first year of this research program (Brownell, et al. [1975]; Garg, et al. [1975b]) and a third will appear (Garg, et al. [1975c]). Oral presentations of the work have been made to several industrial organizations active in the geothermal field and Dr. T. David Riney has visited New Zealand to establish a cooperative effort between S^3 and New Zealand researchers to analyze Wairakei data during Phase II of this effort.

TABLE OF CONTENTS

LIST OF ILLUSTRATIONS

I. INTRODUCTION

Recent interest in the large scale exploitation of geothermal resources provides motivation for the investigation of environmental consequences of geothermal power production. The potential environmental hazards can be grouped into two broad categories - above surface effects (noise, emission of noxious gases) and subsurface or geohydrological effects (land subsidence, induced seismicity, and groundwater contamination). The present research effort is intended to develop a computational capability whereby field information for a specific geothermal system can be used to make predictions of such geohydrological phenomena as land surface subsidence, mixing of geothermal brine into fresh water aquifers, and induced tectonic stresses near faults due to production and reinjection of geothermal fluids.

Land subsidence, sometimes observed during oil field production, is potentially a serious problem in geothermal energy production, particularly of liquid-dominated hydrothermal and geopressured fields. In the Imperial Valley - one of the most promising liquid-dominated geothermal regions in the United States - extensive subsidence could damage irrigation canals and other surface structures. Even if the subsidence is confined to the production area, special measures may be necessary to protect the geothermal extraction and electrical generating equipment. Subsidence is, in general, caused by the compaction of the semi-consolidated and unconsolidated strata of the reservoir as the effective overburden stress is increased due to fluid withdrawal. In some oilfields (e.g., the Wilmington oil field in the Los Angeles basin), injection of water into the formation has been successfully employed to reduce subsidence. Subsidence is potentially a more serious threat in geothermal production due to the much larger volume of fluid required

to produce a given amount of energy. Fluid reinjection, while undoubtedly useful, is not a universal remedy to subsidence, for several reasons. First, while some of the compaction is elastic and may be recovered, it is well known that irreversible pore collapse (permanent deformation) also accompanies fluid withdrawal. Second, due to the nature of the electrical generating process, only a fraction of the produced fluids will be available for reinjection; the reinjected fluid may, of course, be augmented by surface water to make up the volume deficit. Third, reinjection (especially of concentrated brines which are characteristic of some Imperial Valley geothermal anomalies) may not always be practical at (or near) the same horizontal and vertical location as production. Reinjection at a sufficient lateral distance from the producing well may result in uneven surface displacement.

In fields characterized by very high salt concentrations (e.g., the Salton Sea area of Imperial Valley), the residual geothermal brines themselves are generally very concentrated and present a definite disposal problem. It may be economically advantageous to process the fluid to recover some of the dissolved minerals, but in any case substantial amounts of brine will remain. Generally, it is proposed that this residue be reinjected into the ground to avoid polluting surface water bodies (rivers, etc.) and as a partial solution to the problem of land subsidence. On the other hand, care must be taken that the reinjected fluids do not contaminate fresh water aquifers. In this connection we note that hydraulic fracture of the rock may occur during brine reinjection, thereby providing highly permeable channels for the injected brine to penetrate into nearby fresh water aquifers. Furthermore, subsurface fluid injection may, by increasing pore pressures, tend to increase levels of seismic activity. Many geothermal reservoirs (including those in the Imperial Valley and the geopressured systems in the Gulf coast) lie in regions of

extensive faulting - thus, the danger of earthquake triggering cannot be discounted.

All of the geohydrological effects described above involve mechanical interactions between the rock and fluid components. The need to treat rock-fluid interactions also arises in modeling geothermal energy production. As a reservoir is depleted, its pore fluid pressure will decline thereby permitting the pore volume to decrease. Since permeability is very sensitive to porosity changes, the permeability of the geothermal reservoir will diminish with time; changes in permeability can only be predicted by including mechanical interactions between fluid and rock. In addition to mechanical interactions, it is necessary to account for thermal interchange between fluid and rock. Also, the effects of chemistry - both on the thermomechanical properties of the fluid and rock and upon such phenomena as pore blocking and erosion by precipitation and dissolution - need to be modeled, at least in an approximate way.

The general approach, in this three-phase research program, is to construct sophisticated reservoir models, and to develop the required numerical methods to evaluate various phenomena of interest in geothermal systems. The theoretical model, developed within the framework of the Theory of Interacting Continua, describes the thermomechanical response of the rock and fluid (water and/or steam) composite material in terms of the isolated components. The stress-strain equations for the rock matrix are coupled with the diffusion equations for the fluid. The microscale details of the pore/fracture network in the rock are ignored, but the fluid pressures and the stress field in the rock matrix are permitted to assume distinct values within each computational cell for the composite.

A numerical procedure has been derived in Phase I for solving the transport of heat and fluid mass in a "quasi-active" geothermal reservoir. The numerical method is

applicable to single (liquid or vapor) and two-phase (water and steam) in one, two or three dimensions. The quasi-active case is midway in sophistication between the "rigid matrix" model in which all rock properties (e.g., permeability) are treated as functions of position only, and the "fully interactive" case in which the entire rock stress and deformation fields are calculated, along with the heat and fluid flow. In the quasi-active model, the rock thermal properties (heat capacity and thermal conductivity) may be functions of temperature as well as position; the permeability may change with porosity, and the porosity may also vary with position and time, but, at a particular point, the local porosity is assumed to depend only on the local pore pressure. During Phase II, the quasi-active model will be extended to the fully interactive case by supplying constitutive relations for the rock matrix and imposing a static equilibrium conditions (where pore pressure contributes to total stress) at each time step. The basic numerical procedure for treating the fully interactive case has also been developed during Phase I.

The computer model has been applied to simulate single and two-phase flow through bench-scale linear flow models. Comparison of theoretical predictions with the experimental data obtained at Stanford University shows good agreement. Preliminary two-dimensional calculations for a hypothetical hydrothermal reservoir were also carried out during Phase I. These calculations show that production with injection can lead to higher gross power output than production without injection. An illustrative two-dimensional calculation is also presented which describes the land surface subsidence which might accompany the large scale production of a reservoir without reinjection.

To validate the computer model by comparison with field data, it is necessary to have an adequate description of the ambient subsurface environment (stratigraphy, temperature

and pressure distribution, thermomechanical properties of the rock matrix and pore fluids, etc.). Arrangements have been made with the New Albion Resources Company, a wholly owned subsidiary of the San Diego Gas & Electric Company, to provide data from their operations in the Salton Sea area to S^3. The rate of exploitation of geothermal energy in the Salton Sea area, however, is such that sufficient data for full validation of the computer model may not be available for at least another year. The Wairakei geothermal field in New Zealand offers an opportunity for field validation of the model in the near future. A cooperative effort between S^3 and New Zealand researchers has, therefore, been initiated under the Bilateral United States/New Zealand energy research agreement. Computer models developed under this program will be utilized during Phase II to simulate the gross production and subsidence history for the Wairakei geothermal field.

The progress made during Phase I is described in the following sections. Section II treats the general problem of multi-phase fluid and heat flow in a deforming porous rock matrix, and constitutive relations for the multi-phase water and rock. Numerical solution of the fluid-flow and rock response equations is discussed in Section III. Application of the fluid flow model to simulate single and two-phase flow through laboratory models, and preliminary two-dimensional production/injection calculations for a hypothetical hydrothermal reservoir are described in Section IV. Application of the rock response model to calculate surface deformations (vertical and horizontal) are also discussed in Section IV. Section V deals with seismic data compilation and geochemical effects. Finally, future plans are discussed in Section VI.

II. DEVELOPMENT OF THE THEORETICAL MODEL

There have been many studies emphasizing heat and mass transfer in porous media; in the main, these investigations deal with single phase (liquid) flow in the limit of the Boussinesq approximation (see, e.g., Wooding [1957, 1963], Donaldson [1962], Elder [1967a, 1967b], Bories and Combarnous [1973]). Recent interest in the simulation of geothermal reservoirs has led several investigators to the consideration of two-phase (water/steam) flow in porous media (see, e.g., Donaldson [1968], Mercer, et al. [1974], Brownell, et al. [1975]). Geothermal basins are, in general, complex thermo-mechanical systems containing unconsolidated and semi-consolidated materials and fractured rock masses. The production rate of geothermal reservoirs may depend on, among other variables, compaction of unconsolidated rocks (as in geopressured reservoirs). To be generally useful, a theoretical model should be able to account for the following effects: (1) thermally induced fluid convection, (2) pore (or fracture) collapse and subsidence due to fluid withdrawal, and (3) effect of pore collapse on fluid withdrawal.

We are thus concerned with a fully interacting rock-fluid system. These interactions involve mass, momentum and energy transfer, variable porosity and permeability. In addition, the system may be anisotropic and inhomogeneous in the large. General balance laws and constitutive relations incorporating the various interactions in a solid-fluid mixture have previously been developed by Morland [1972] and Garg, et al. [1971, 1973, 1975a]. For geothermal reservoir applications where fluid velocities are low and times of interest are long, it is possible to considerably simplify the general balance laws. Permissible simplifications are discussed in detail by Brownell, et al. [1975]. Briefly, in geothermal applications, it is possible to ignore (1) the inertia terms in

the momentum equations, and (2) the pressure work and viscous diffusion terms in the energy equations. Furthermore, the fluid and the solid may be assumed to be in local thermal equilibrium. Justification for the latter is given by Nayfeh, et al. [1975]. This simplified system of governing equations is similar to the heuristic formulations of two-phase flow (excluding solid motion) developed by Donaldson [1968] and Mercer, et al. [1974].

The simplified balance laws and the appropriate constitutive relations are discussed in the following subsections. Section 2.1 describes the balance laws for the two-phase flow through deformable porous media. Constitutive relations for the geothermal fluids (water/steam) and the rock matrix are given in Sections 2.2 and 2.3, respectively.

2.1 BALANCE LAWS

Assuming that (1) the rock matrix undergoes only small deformations, (2) capillary pressure is negligible, (3) liquid water and water vapor are in local pressure and thermal equilibrium ($P_\ell = P_v = P$, $T_\ell = T_v = T$), (4) fluid (water/water vapor) and rock matrix are in local thermal equilibrium ($T_s = T$), (5) and the fluid motion is governed by Darcy's law, the equations expression mass, momentum and energy balance can be written as follows:

Mass

Liquid:

$$\left[\frac{\partial}{\partial t} + (\underline{v}_\ell - \underline{v}_s)\cdot\nabla\right] [\phi(1-S)\rho_\ell] + \phi(1-S)\rho_\ell \nabla\cdot\underline{v}_\ell = -\dot{m} \quad (2.1)$$

Vapor:

$$\left[\frac{\partial}{\partial t} + (\underline{v}_v - \underline{v}_s)\cdot\nabla\right] [\phi S\rho_v] + \phi S\rho_v \nabla\cdot\underline{v}_v = \dot{m} \quad (2.2)$$

Solid:

$$\dot{\varepsilon} = \nabla \cdot \underline{v}_s \tag{2.3}$$

Momentum

Liquid:

$$\underline{v}_\ell - \underline{v}_s = - \frac{R_\ell k}{\phi(1-S)\mu_\ell} [\nabla P - \rho_\ell \underline{g}] \tag{2.4}$$

Vapor:

$$\underline{v}_v - \underline{v}_s = - \frac{R_v k}{\phi S \mu_v} [\nabla P - \rho_v \underline{g}] \tag{2.5}$$

Solid:

$$-\nabla[(1-\phi)P_s + \phi P] + \text{div } \underline{\underline{S}} + [(1-\phi)\rho_s + \phi(1-S)\rho_\ell + \phi S \rho_v] \underline{g} = 0 \tag{2.6}$$

Energy

Rock-liquid-vapor mixture:

$$\frac{\partial}{\partial t} [(1-\phi)\rho_s E_s + \phi(1-S)\rho_\ell E_\ell + \phi S \rho_v E_v] + \nabla \cdot [\phi(1-S)\rho_\ell E_\ell (\underline{v}_\ell - \underline{v}_s) + \phi S \rho_v E_v (\underline{v}_v - \underline{v}_s)] = \nabla \cdot [\kappa_m \nabla T] \tag{2.7}$$

where

E_i = Internal energy of ith phase [i = s (solid, i = ℓ (liquid), i = v (vapor), i = f (fluid)].

$\underline{g}$ = Acceleration due to gravity.

k = Rock permeability.

$\dot{m}$ = Mass transfer rate from liquid to vapor due to phase change.

$P_i (=P)$ = Pressure ($i = \ell, v, f$).

P_s = Solid pressure.

$R_\ell (R_v)$ = Relative permeability for liquid (vapor).

S = Relative vapor volume [$= V_v/(V_v + V_\ell)$].

$\underset{\sim}{S}$ = Deviatoric stress tensor for porous rock.

t = Time.

$T_i (=T)$ = Temperature ($i = s, \ell, v, f$).

$\underline{v}_i$ = Velocity of ith phase ($i = s, \ell, v$).

$V_v (V_\ell)$ = Vapor (liquid) volume.

$\underline{x}$ = Space vector.

$\dot{\epsilon}$ = Bulk volumetric strain-rate for rock.

κ_i = Thermal conductivity of ith phase ($i = s, \ell, v$).

κ_m = Mixture (solid-liquid-vapor) thermal conductivity.

μ_i = Viscosity ($i = \ell, v$).

ρ_i = Density ($i = s, f, \ell, v$).

ϕ = Porosity.

A few remarks are here in order concerning the basic assumptions and the balance laws. The mass balance law for the rock matrix, Eq. (2.3), follows directly from the small strain assumption (1). The restriction to small strains is entirely appropriate for geothermal reservoirs wherein the matrix deformation is expected to be a small percentage of the reservoir thickness. For water-steam systems, the capillary pressure is less than a bar, and is, therefore, likely to be insignificant in comparison with the pressure changes induced by production/injection. Capillary pressure may be included in the balance laws by modifying the pressure equilibrium

relation ($P_\ell = P_v = P$). The momentum balance relation, Eq. (2.6), for the solid matrix merely states that the reservoir behaves in a quasi-static manner during production/injection. Finally, it is to be noted that the assumption of thermal equilibrium ($T_\ell = T_v = T_s = T$) obviates the need to consider energy balance separately for each constituent.

2.2 CONSTITUTIVE RELATIONS FOR GEOTHERMAL FLUIDS (WATER/STEAM)

For computational purposes, it is convenient to eliminate the separate density (ρ_ℓ, ρ_v) and energy (E_ℓ, E_v) fields for liquid and vapor and to employ instead mixture (liquid-vapor) density (ρ_f) and energy (E_f) fields:

$$\rho_f = S\rho_v + (1-S)\,\rho_\ell \tag{2.8}$$

$$E_f = \frac{(1-S)\rho_\ell\, E_\ell + S\rho_v\, E_v}{\rho_f} \tag{2.9}$$

Introducing the "steam quality" Q

$$Q = M_v/(M_\ell + M_v) \tag{2.10}$$

ρ_ℓ, ρ_v, E_ℓ, and E_v can be expressed in terms of ρ_f, E_f, Q, S and δ:

$$\begin{aligned}
\rho_\ell &= \rho_f\left[\frac{1-Q}{1-S}\right] \\
\rho_v &= \rho_f\left[\frac{Q}{S}\right] \\
\rho_\ell E_\ell &= \rho_f\, E_f\left[\frac{(1-Q)(1-\psi Q)}{1-S}\right] \\
\rho_v E_v &= \rho_f\, E_f\left\{\frac{Q[1+\psi(1-Q)]}{S}\right\}
\end{aligned} \tag{2.11}$$

where

ψ = δ/E_f,

$M_\ell (M_v)$ = Liquid (vapor) mass per unit volume,

δ = Heat of vaporization

Substituting for ρ_ℓ, ρ_v, E_ℓ, and E_v from Eqs. (2.11) into Eqs. (2.1) - (2.7) gives the balance relations in the desired form.

The modified system of balance equations contains liquid and vapor viscosities, relative vapor volume, steam quality, and latent heat of vaporization in addition to fluid density (ρ_f), internal energy (E_f) and pressure (P). Furthermore, specification of mixture (solid-liquid-vapor) thermal conductivity (κ_m) requires the knowledge of liquid (κ_ℓ) and vapor (κ_v) conductivities. It was, therefore, necessary to construct a fairly general tabular equation of state for water. Given fluid density (ρ_f) and internal energy (E_f), the equation of state subroutines used in the simulation code yield pressure (P), derivatives of pressure with respect to ρ_f and E_f, steam volume fraction (S) and quality (Q), fluid temperature (T), derivatives of temperature with respect to ρ_f and E_f, latent heat of vaporization (δ) and its derivatives with respect to ρ_f and E_f. This description is valid up to ultra-high pressures (several megabars), and temperatures up to 3000°C. Figures 2.1 and 2.2 show the equation of state data in the pressure-volume and density-energy planes. The equation of state subroutines also give liquid and vapor viscosities (μ_ℓ, μ_v) and thermal conductivities (κ_ℓ, κ_v) as functions of ρ_f and E_f; these data are, however, valid up to only pressures less than 1 kbar and temperatures less than 800°C.

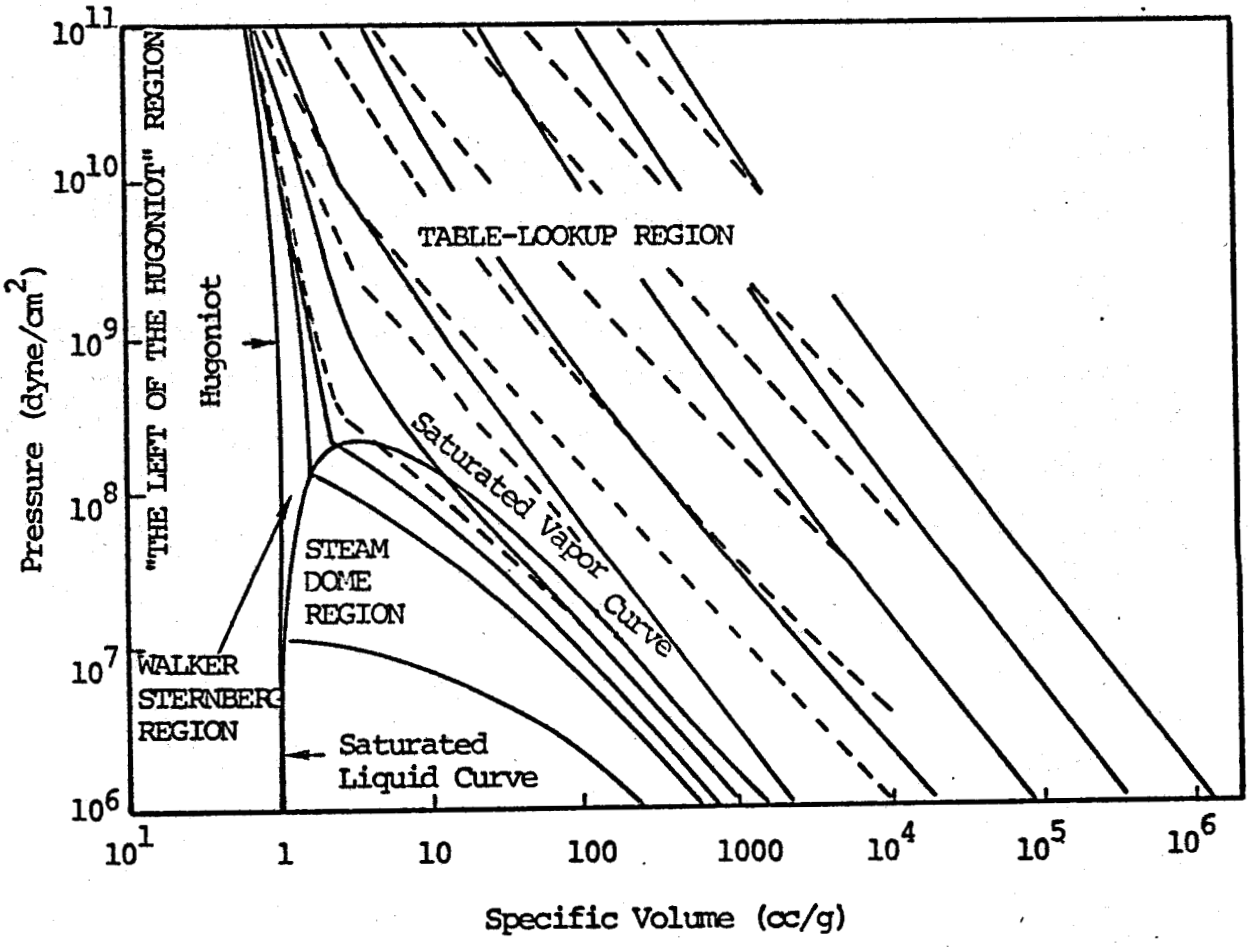

Figure 2.1. Isentropes (solid) and iso-energy (dashed) curves in the pressure-volume plane.

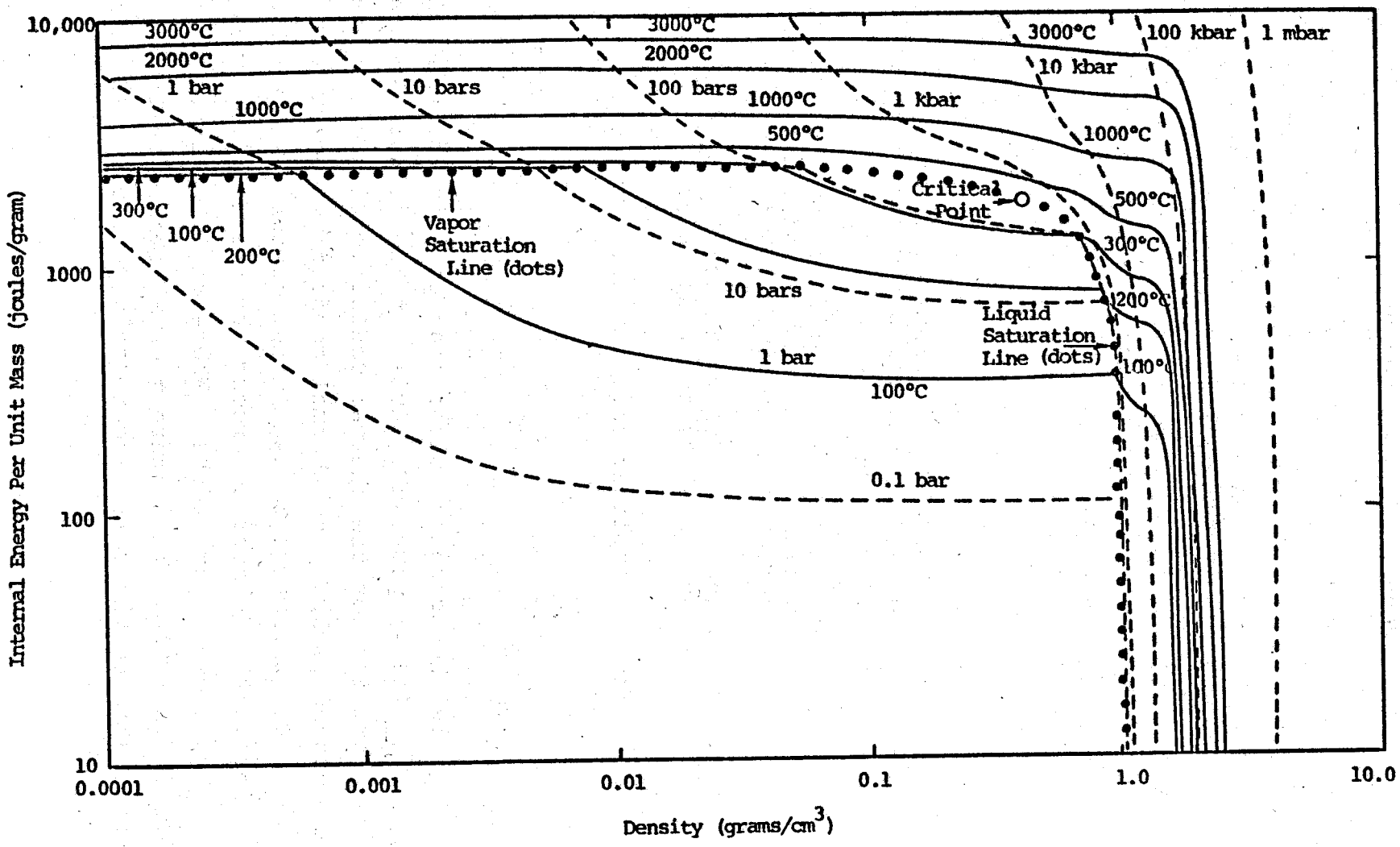

Figure 2.2. Isobars (dashed) and isotherms (solid) in the density-energy plane.

2.3 CONSTITUTIVE RELATIONS FOR THE ROCK MATRIX

We need to prescribe the following functions [Garg, et al. 1975b; Brownell, et al. 1975] for the rock matrix:

$T_s(E_s)$ ~ Dependence of rock temperature on rock internal energy.

$\kappa_m(\kappa_i,\phi,S)$ ~ Dependence of the mixture (solid-liquid-vapor) conductivity on κ_i, ϕ and S.

$\kappa_s(T)$ ~ Dependence of thermal conductivity on temperature.

$k(\phi)$ ~ Dependence of permeability on porosity ϕ.

$R_{\ell,v}(S,T)$ ~ Dependence of relative liquid and vapor permeabilities on steam saturation and temperature.

$\underset{\sim}{\sigma}^s(\underset{\sim}{\varepsilon},T_s)$ ~ [$= -(1-\phi)P_s \underset{\sim}{I} + \underset{\sim}{S}$] dependence of rock matrix stress tensor upon rock strain tensor ($\underset{\sim}{\varepsilon}$) and temperature.

$\phi(\underset{\sim}{\sigma}^s,P,T)$ ~ Dependence of rock porosity upon the stress state and temperature.

For geothermal applications, it will suffice to assume that

$$E_s = C_{vs}\, T_s \tag{2.12}$$

where C_{vs} is the constant volume heat capacity of the solid. Ramey, et al. [1974] present a review of the measurements and empirical formulas for the thermal conductivities of dry and fluid-saturated rocks. The thermal conductivity of most rocks decreases with an increase in temperature. Thermal conductivities of fluid-saturated rocks are two to five times greater than those of dry rocks. Where detailed experimental data are unavailable, the mixture thermal conductivity κ_m may be approximated by the following relationship due to Budiansky [1970]:

$$(1-\phi)\left[\frac{2}{3}+\frac{1}{3}\left(\frac{\kappa_s}{\kappa_m}\right)\right]^{-1}+\phi\left\{(1-S)\left[\frac{2}{3}+\frac{1}{3}\left(\frac{\kappa_\ell}{\kappa_m}\right)\right]^{-1}+S\left[\frac{2}{3}+\frac{1}{3}\left(\frac{\kappa_v}{\kappa_m}\right)\right]^{-1}\right\}=1 \tag{2.13}$$

The rock permeability k is a complex function of rock and fluid stresses (see, e.g., Brace [1972]). For the sake of simplicity, we will postulate that this dependence is primarily exhibited through changes in porosity ϕ. In particular, k will be assumed to be given by

$$k = k_0\left(\frac{\phi}{\phi_0}\right)^n\left(\frac{1-\phi_0}{1-\phi}\right)^m \tag{2.14}$$

where n and m are empirically determined constants. Note that $n = 3$, $m = 2$ yields the classical Carman-Kozeny relation (see, e.g., Scheidegger [1963]). Sufficient data are unavailable to determine the dependence of relative permeabilities ($R_{\ell,v}$) on temperature; it will be, therefore, assumed that the relative permeabilities are functions only of vapor saturation S. In particular, the relative permeabilities may be represented by the equations of Corey, et al. [1956].

$$\begin{aligned} R_\ell &= (S_\ell^*)^4 \\ R_v &= (1-S_\ell^{2*})\ (1-S_\ell^*)^2 \end{aligned} \tag{2.15}$$

where

$$\begin{aligned} S_\ell^* &= (S_\ell - S_{\ell r})/(1-S_{\ell r}-S_{vr}) \\ S_\ell &= 1 - S \end{aligned} \tag{2.16}$$

Here $S_{\ell r}$ (S_{vr}) is the irreducible liquid (vapor) saturation, and S_ℓ^* is the volumetric liquid saturation normalized with

respect to the mobile fluid saturation in the pore space. Note that for $S_\ell < S_{\ell r}$, $R_\ell = 0$ and $R_v = 1$; and for $S_\ell > (1-S_{vr})$, $R_\ell = 1$ and $R_v = 0$. It is appropriate to point out here that the method of solution outlined in the next section does not depend upon the specific functional forms of Eqs. (2.12) through (2.16); as a matter of fact, the computer code (incorporating the method of solution) is configured so as to accept any prescribed functional forms for $T_s(E_s)$, $\kappa_s(T)$, $\kappa_m(\kappa_i, \phi, S)$, $k(\phi)$ and $R_{\ell,v}(S,T)$. In the remainder of this subsection, we shall consider the constitutive relations for $\underset{\sim}{\sigma}^s$ and ϕ.

The bulk strain-rate tensor for rock $\dot{\underset{\sim}{\varepsilon}}$ is given by:

$$\dot{\underset{\sim}{\varepsilon}} = \frac{1}{2} [\nabla \underline{v}_s + (\nabla \underline{v}_s)^t] = \frac{\dot{\varepsilon}}{3} \underset{\sim}{I} + \dot{\underset{\sim}{e}} \tag{2.17}$$

where $\dot{\underset{\sim}{e}}$ denotes the deviatoric part of the strain-rate tensor. Bulk volumetric strain ε is related to the rock grain (or effective) volumetric strain ε^e through the relation:

$$\varepsilon^e = \frac{\rho_{0s}}{\rho_s} - 1 = \left(\frac{1-\phi}{1-\phi_0}\right) (1 + \varepsilon) - 1 \tag{2.18}$$

The rock grain may be assumed to be a linear thermoelastic material over the range of temperatures and pressures encountered in geothermal reservoirs.

$$P_s = -K_s (\varepsilon^e - 3 \eta_s T_s) \tag{2.19}$$

where K_s (η_s) denotes the bulk modulus (coefficient of linear thermal expansion) for the rock grain. Additionally, we will postulate that the shear stresses $\underset{\sim}{S}$ are linearly related to shear strains $\underset{\sim}{e}$ through Hooke's law:

$$\underset{\sim}{S} = 2 \mu_p \underset{\sim}{e} \tag{2.20}$$

where μ_p is the shear modulus of the porous rock. It should

be pointed out here that the methods of numerical solution, outlined in Section III, do not depend upon the specific functional forms, Eqs. (2.19) and (2.20).

Porosity ϕ depends in a complex manner on the current state of stress ($\underset{\sim}{\sigma}^s$, P), stress history, temperature and the rock type. Consolidated rocks generally exhibit greater compaction at elevated temperatures than they do at lower temperatures; the effect of temperature is not, however, so significant in loose or unconsolidated sands. Shear stresses $\underset{\sim}{S}$, depending upon the rock type, may contribute to compaction, may lead to dilatancy, or may have no significant effect upon ϕ. Let us consider the case when ϕ does not appreciably depend upon $\underset{\sim}{S}$; in this case ϕ (at constant T) can be expressed as a function of $(P_c - P)$ and P [Garg, et al. 1975a]:

$$\phi = \phi\ (P_c - P,\ P) \tag{2.21}$$

where

$$P_c = (1-\phi)\ P_s + \phi P\ .$$

If P is identically zero, then Eq. (2.21) simplifies to

$$\phi = \phi\ (P_c) \tag{2.22}$$

The general form of the function $\phi(P_c)$ is shown in Fig. 2.3. For $P_c < P_e$, pore collapse is reversible; for $P_1 \geq P_c \geq P_e$, irreversible pore collapse takes place. Specific functional forms for $\phi(P_c - P,\ P)$ may be developed on the basis of either laboratory or field data (see, e.g., Garg, et al. [1975a]).

For small deformations (characteristic of geothermal problems), porosity ϕ depends to a close approximation only upon $P_c - P$.

$$\phi = \phi\ (P_c - P) \tag{2.23}$$

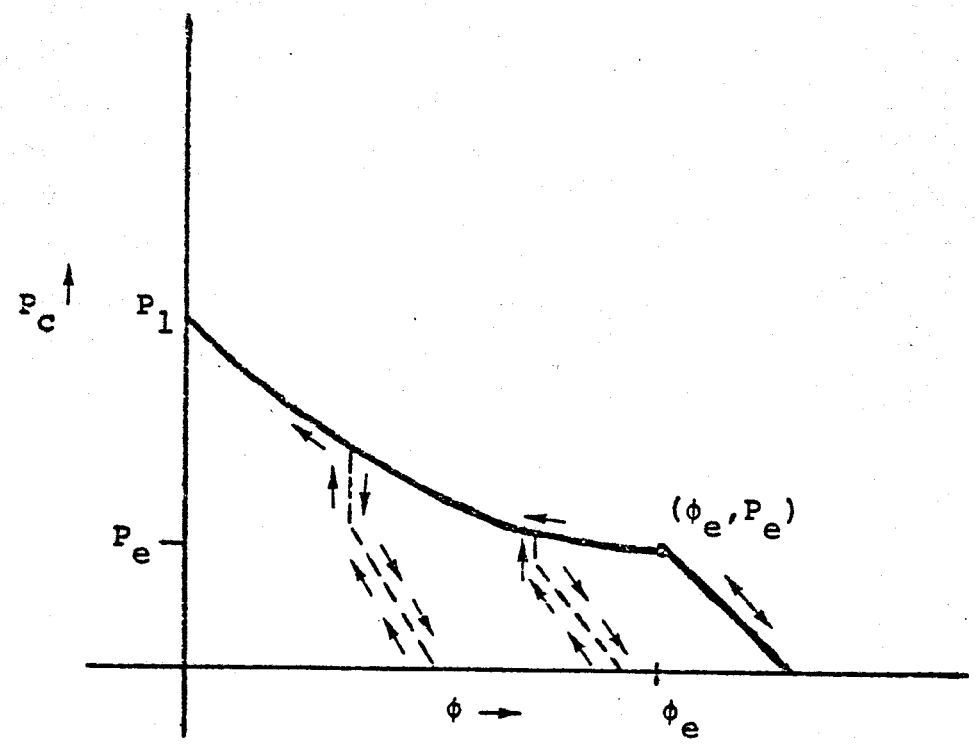

Figure 2.3. Reversible and irreversible pore collapse ($P \equiv 0$, $P_c \neq 0$). Elastic loading and unloading ($P_c \leq P_e$), irreversible loading ($P_c \geq P_e$); — unloading and reloading.

This last result can be derived in a straightforward manner from the analysis of Garg and Nur [1973]. Equation (2.23) can be rewritten as [Garg and Nur, 1973]:

$$\phi = \phi_0 \, [1 + \alpha(P_c - P)] \tag{2.24}$$

where

$$\alpha \equiv \alpha \, (P_c - P) = \frac{1}{\phi_0}\left[\frac{1}{K_S} - \frac{1-\phi_0}{K}\right] \tag{2.25}$$

Here $K(P_c-P)$ is the bulk modulus of the porous rock and has different values during loading (increase in effective pressure $P_c - P$) and unloading (decrease in effective pressure $P_c - P$).

The theoretical model discussed above requires C_{vs}, κ_s, k, $R_{\ell,v}$, ϕ, μ_p, K, K_s and η_s as empirically determined input functions. Most of these properties can be obtained from standard laboratory tests on cores obtained from the reservoir in question. The reservoir behavior is, however, frequently governed by fractures, formation inhomogeneities, and other large scale features such as faults. In particular, the producibility and compaction behavior of a geothermal reservoir will be profoundly influenced by the presence of fractured rock masses. It, therefore, becomes important to supplement the laboratory measurements by suitable field data. Permeability k and relative permeabilities $R_{\ell,v}$ are best determined from well flow data (this is a standard practice in petroleum reservoir engineering). Also, bulk and shear moduli (K, μ_p) of reservoir rocks should be obtained from seismic measurements.

III. NUMERICAL TECHNIQUES

The theoretical model, outlined in Section II, describes the thermomechanical response of the rock and fluid (water and/or steam). The stress-strain equations for the rock matrix are coupled with the diffusion equations for the fluid. During Phase I of this three-phase research program, a numerical procedure was developed for solving the transport of heat and fluid mass in a "quasi-active" geothermal reservoir in one, two or three dimensions. The method properly treats the effects of phase changes (liquid ⇄ vapor) within the pores of the reservoir rock. The quasi-active case is midway in sophistication between the "rigid-matrix" model in which all rock properties (porosity, permeability, thermal conductivity, etc.) are treated as functions of position only and the "fully interactive" case (in which the entire rock stress and deformation fields are calculated along with the heat and fluid flow). In the quasi-active model, the rock thermal properties (heat capacity and thermal conductivity) may be functions of temperature as well as position; the permeability may change with porosity, and the porosity may also vary with position and time, but at a particular point, the local porosity is assumed to depend only on the local pore pressure. During Phase II of the research program, the quasi-active model will be extended to the fully interactive case by coupling the fluid diffusion equations with the stress-strain equations for the rock matrix. The basic numerical procedure for treating the fully interactive case has also been developed during Phase I. Section 3.1 discusses the quasi-active fluid-flow model. The rock response model is described in Section 3.2. Finally, the procedure for the development of "integrated rock-fluid response model" is outlined in Section 3.3.

3.1 THE FLUID-FLOW MODEL

The governing equations for the "quasi-active" geothermal reservoir consist of separate mass and momentum balance laws for the liquid (Eqs. (2.1) and (2.4)) and vapor (Eqs. (2.2) and (2.5)), and an energy balance law for the rock-liquid-vapor mixture (Eq. (2.7)). The explicit presence of velocities $\underline{v}_\ell$ and $\underline{v}_v$ (note that $\underline{v}_s \equiv 0$ for the quasi-active reservoir) in the mass and energy balance equations may be eliminated by substituting for $\underline{v}_\ell$ and $\underline{v}_v$ from Eqs. (2.4) and (2.5). The mass transfer term in the mass balance laws for the liquid and vapor components may be eliminated by summing Eqs. (2.1) and (2.2). Thus, the modified system of mass (1 equation) and energy (1 equation) balance equations together with the thermal equilibrium relation (1 equation) constitute a set of three equations for three unknowns mixture (liquid-vapor) density, mixture internal energy, and solid internal energy. For the sake of convenience, we will utilize a slightly different notation here than that employed in Section II. In the present notation the mass, energy and thermal balance laws are:

Mass:

$$\frac{\partial}{\partial t}[\phi\rho] = \dot{m} + \nabla \cdot \left[k\left([\alpha_L\rho]\left[\nabla P - \rho_L \vec{g}\right] + [\alpha_v\rho]\left[\nabla P - \rho_v \vec{g}\right]\right)\right] \tag{3.1}$$

Energy:

$$\frac{\partial}{\partial t}[E_s + \phi E] = \dot{e} + \nabla \cdot \left[k\left([\beta_L E]\left[\nabla P - \rho_L \vec{g}\right] + [\beta_v E]\left[\nabla P - \rho_v \vec{g}\right]\right) + \bar{K}\,\nabla T\right] \tag{3.2}$$

Thermal Equilibrium:

$$T_s = T \ , \tag{3.3}$$

where

	S = 0 (all liquid)	0 < S < 1 (multiphase)	S = 1 (all vapor)
α_L	$1/\mu$	$\frac{1-Q}{1-S}\frac{R_L}{\mu_L}$	0
α_v	0	$\frac{Q}{S}\frac{R_v}{\mu_v}$	$1/\mu$
β_L	$1/\mu$	$\alpha_L[1-QE_{vap}/E]$	0
β_v	0	$\alpha_v[1+(1-Q)E_{vap}/E]$	$1/\mu$

and

E = Bulk fluid internal energy per unit fluid volume.

E_{vap} = Latent heat of vaporization per unit fluid volume.

E_S = Solid internal energy per unit total volume.

ρ = Bulk fluid density.

ρ_v = Vapor phase density = $\rho Q/S$.

ρ_L = Liquid phase density = $\rho(1-Q)/(1-S)$.

Q = Steam quality.

S = Steam saturation.

$\mu(\mu_L;\mu_v)$ = Bulk fluid (liquid; vapor phase) viscosity.

$R_v(R_L)$ = Relative vapor (liquid) permeability.

k = Absolute solid permeability.

$\bar{\kappa}$ = Mixture (rock-liquid-vapor) heat conductivity.

ϕ = Porosity.

P = Pressure.

T = Fluid temperature.

T_S = Solid temperature.

$\vec{g}$ = Acceleration of gravity.

$\dot{m}$ = Local fluid mass source/sink rate.

$\dot{e}$ = Local heat source/sink rate.

The balance laws expressed in Eqs. (3.1) and (3.3) are adjoined by the following constitutive relations:

$P, T, Q, S, \mu_L, \mu_v, E_{vap}, \kappa_L, \kappa_v$ = functions of (ρ,E)

T_s = function of E_s

R_L, R_v = function of S

ϕ = function of P

k = function of ϕ

For details of constitutive relations, reference is made to Section II.

Since the times of interest in geothermal reservoirs are long, and the governing equations are highly nonlinear, it is necessary to employ an implicit (in time) and iterative finite-difference procedure. The first order finite-difference analog of the Eqs. (3.1) - (3.3) in the time domain is:

Mass:

$$\frac{\phi^{n+1}\rho^{n+1} - \phi^{n}\rho^{n}}{\Delta t} = \dot{m}^{n+\frac{1}{2}} + \nabla \cdot \left[k^{n} \left(\left[\alpha_{L}^{n} \rho^{n+1} \right] \left[\nabla P^{n+1} - \rho_{L}^{n} \vec{g} \right] + \left[\alpha_{v}^{n} \rho^{n+1} \right] \left[\nabla P^{n+1} - \rho_{v}^{n} \vec{g} \right] \right) \right]$$

Energy:

$$\frac{E_{s}^{n+1} + \phi^{n+1}E^{n+1} - E_{s}^{n} - \phi^{n}E^{n}}{\Delta t} = \dot{e}^{n+\frac{1}{2}} + \nabla \cdot \left[k^{n} \left(\left[\beta_{L}^{n} E^{n+1} \right] \left[\nabla P^{n+1} - \rho_{L}^{n} \vec{g} \right] + \left[\beta_{v}^{n} E^{n+1} \right] \left[\nabla p^{n+1} - \rho_{v}^{n} \vec{g} \right] \right) + \overline{K}^{n} \nabla T^{n+1} \right] \tag{3.5}$$

Thermal Equilibrium:

$$T_{s}^{n+1} = T^{n+1} \tag{3.6}$$

where the superscript n denotes the value of the superscripted variable at $t = n\Delta t$. A convenient method for solving Eqs. (3.4) through (3.6) in the space domain is the so-called Alternating Direction Implicit (ADI) method; ADI allows one to reduce a multi-dimensional (2D or 3D) problem to a series of one-dimensional problems. To illustrate the ADI method, it is convenient to consider the linear heat conduction equation in two dimensions (planar geometry):

$$\frac{\partial T}{\partial t} = K \left(\frac{\partial^{2} T}{\partial x^{2}} + \frac{\partial^{2} T}{\partial y^{2}} \right) \tag{3.7}$$

The first order implicit (time) finite difference analog of Eq. (3.7) is

$$\frac{T^{n+1} - T^{n}}{\Delta t} = K \left(\frac{\partial^{2}}{\partial x^{2}} \left[T^{n+1} \right] + \frac{\partial^{2}}{\partial y^{2}} \left[T^{n+1} \right] \right) \tag{3.8}$$

The ADI technique replaces Eq. (3.8) by two one-dimensional problems:

$$\frac{{}^{k+1}T^{n+1} - T^{n}}{\Delta t} = K\left(\frac{\partial^2}{\partial x^2}\left[{}^{k+1}T^{n+1}\right] + \frac{\partial^2}{\partial y^2}\left[{}^{k}T^{n+1}\right]\right)$$

$$\frac{{}^{k+2}T^{n+1} - T^{n}}{\Delta t} = K\left(\frac{\partial^2}{\partial x^2}\left[{}^{k+1}T^{n+1}\right] + \frac{\partial^2}{\partial y^2}\left[{}^{k+2}T^{n+1}\right]\right) \qquad (3.9)$$

where the pre-superscript k denotes the kth iteration. Given T^n and ${}^{k}T^{n+1}$, one first solves for ${}^{k+1}T^{n+1}$ from Eq. (3.9a); T^n and ${}^{k+1}T^{n+1}$ are then employed in Eq. (3.9b) to solve for ${}^{k+2}T^{n+1}$. Note that ${}^{k+1}T^{n+1}$ in Eq. (3.9a), and ${}^{k+1}T^{n+1}$ in Eq. (3.9b) appear as merely source terms. This iterative procedure is repeated until some preset convergence criterion is met. The application of ADI to solve the system of balance Eqs. (3.4 - 3.6) involves essentially (apart from quite involved algebra) the steps outlined above.

The ADI method is particularly convenient for treating complex geometries. Figure 3.1a shows a multiply-connected two-dimensional region; the corresponding computational grid is shown in Fig. 3.1b. ADI segments in x and y directions are given in Figs. 3.1c and 3.1d, respectively. The psuedo 1D field equation of the above type, Eq. (3.9a) or (3.9b), for the (k+1)th approximation to the solution is solved for the 1D block illustrated in Fig. 3.1e.

The numerical scheme has been incorporated into a finite-difference code QUAGMR (Quasi-Active Geothermal Model Reservoir). The QUAGMR code possesses considerable flexibility, as far as problem geometry, heterogeneous matrix properties, and boundary conditions are concerned. The present version of the code can treat the following geometries:

- 1D Slab, Cylindrical or Spherical
- 2D Planar or Axisymmetric
- 3D Cartesian

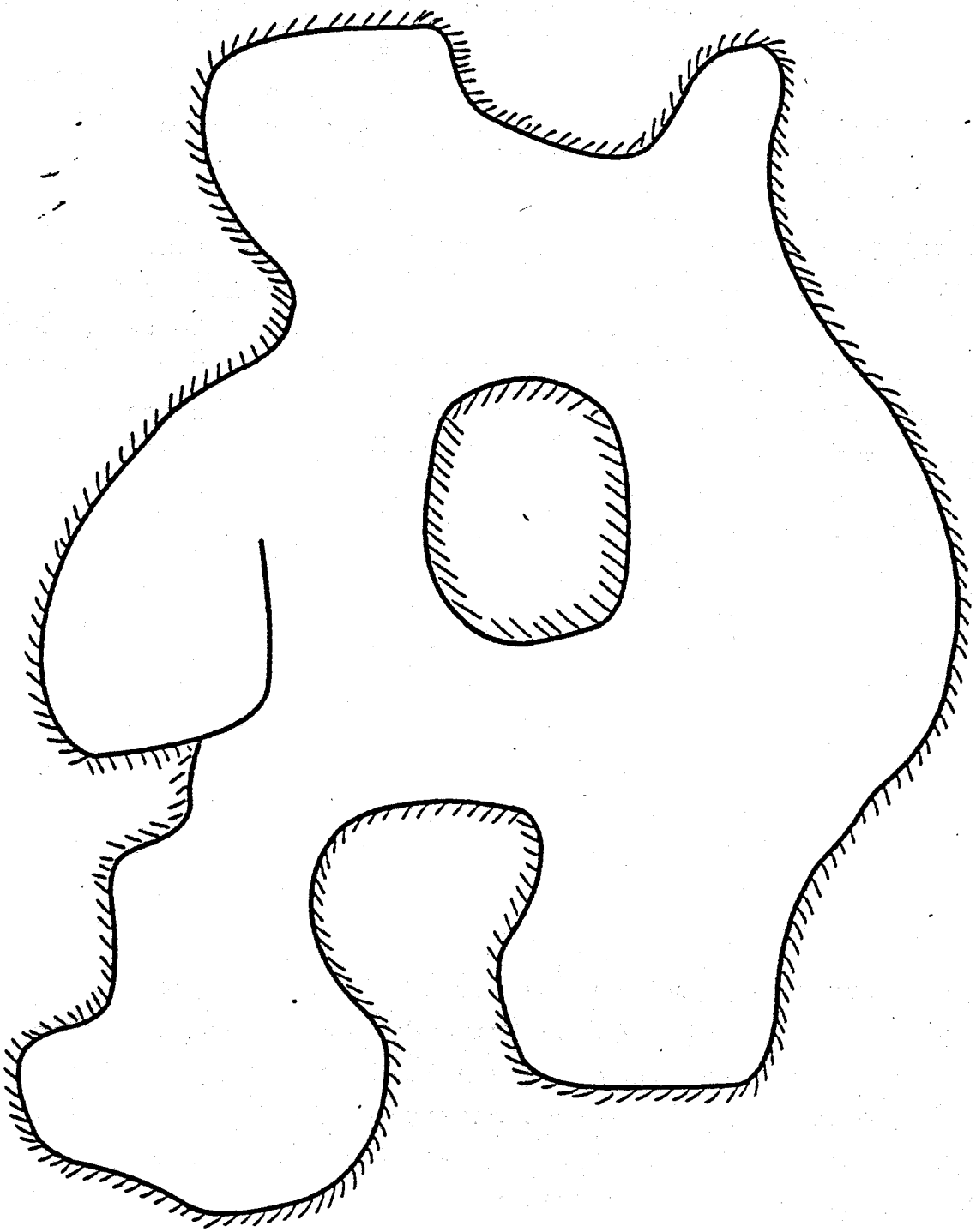

Figure 3.1a. Representation of a complex problem geometry.

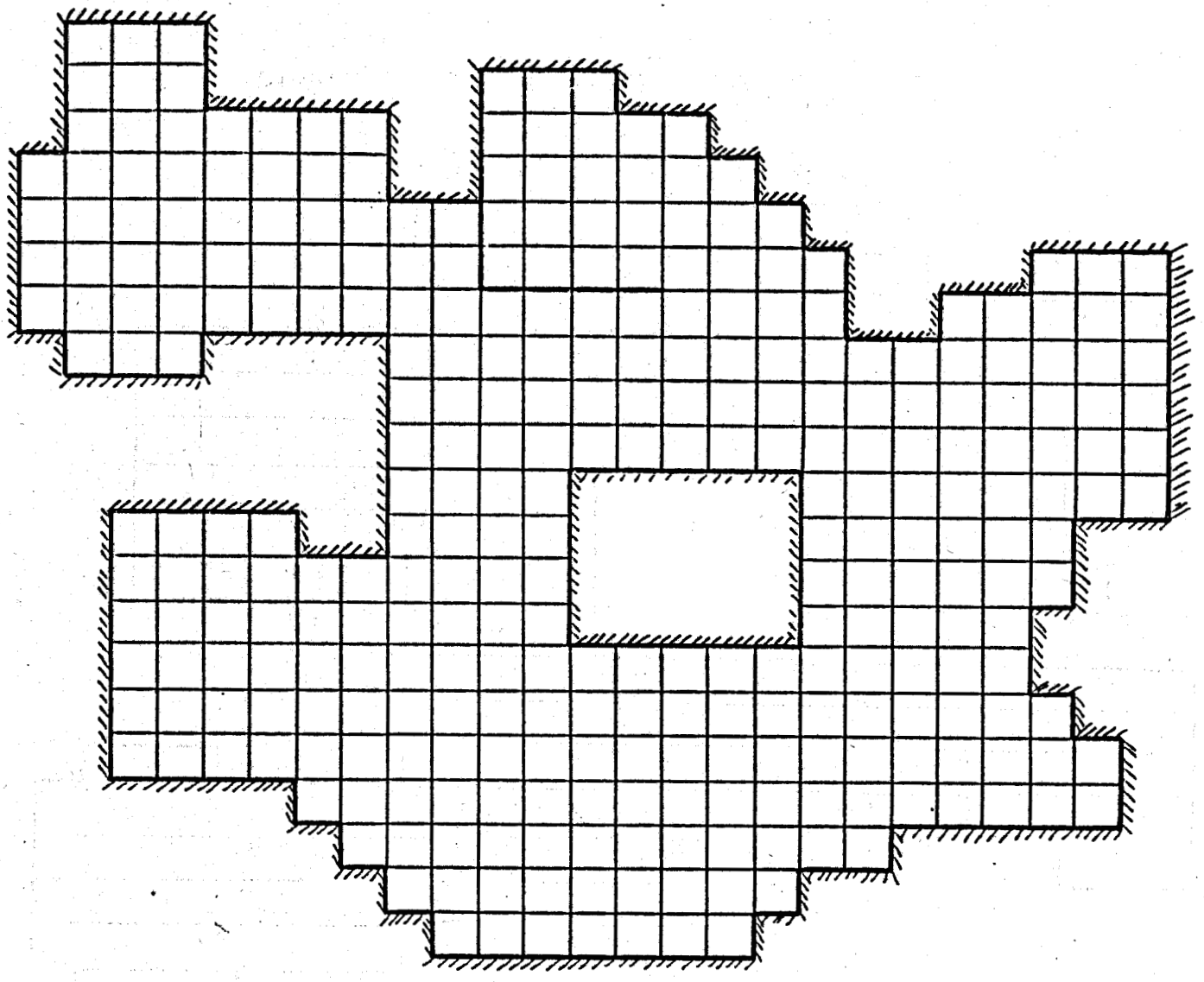

Figure 3.1b. Computational grid for problem geometry.

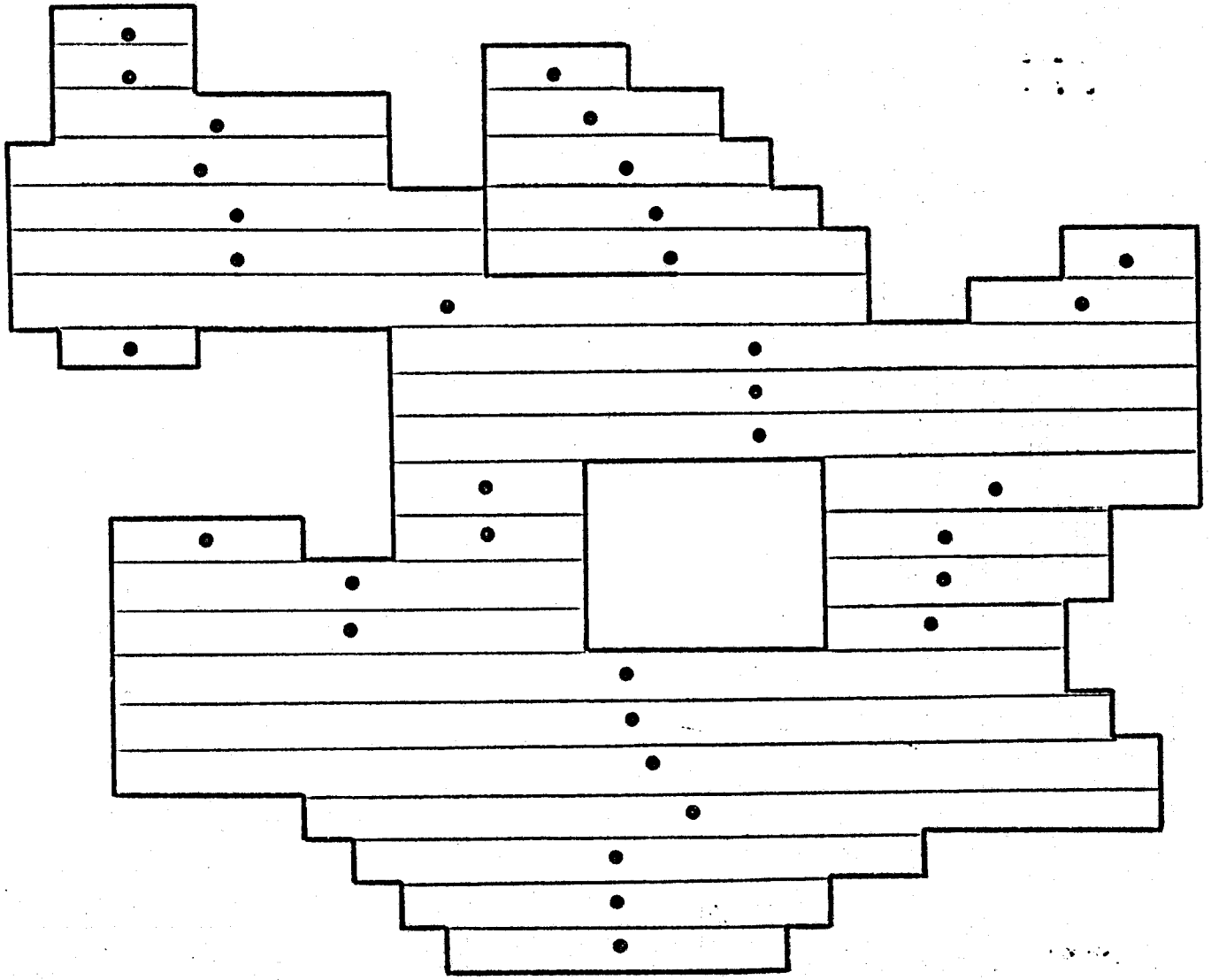

Figure 3.1c. X direction ADI segments.

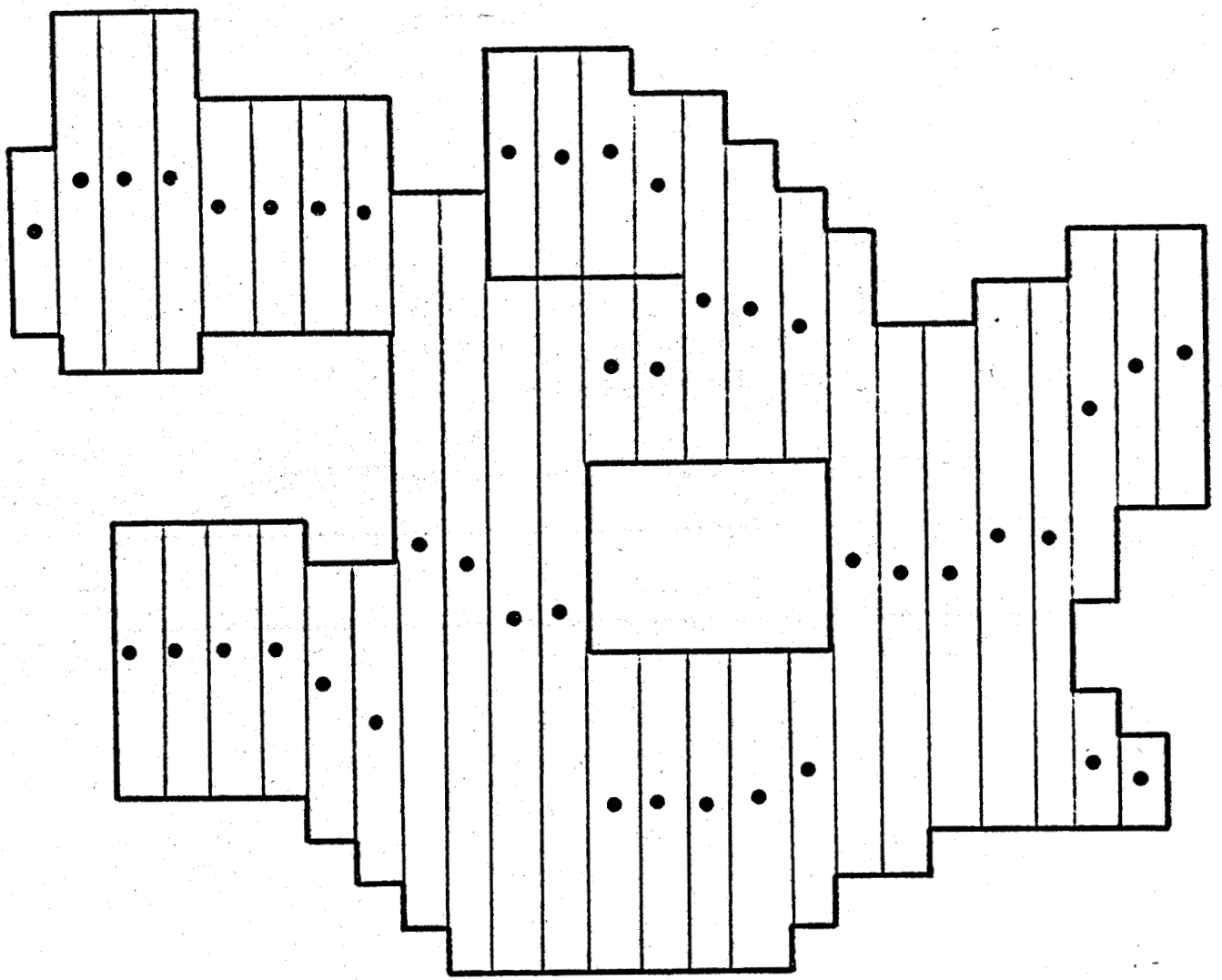

Figure 3.1d. Y direction ADI segments.

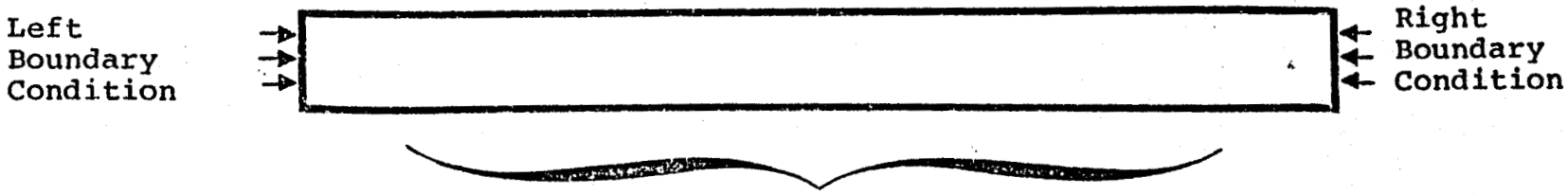

Figure 3.1e. 1D block.

Each computational zone may contain a different rock type. Rock types are characterized by the following properties:

- Density
- Porosity
- Directional absolute permeabilities
- Relative permeability functions
- Heat capacity
- Thermal conductivity
- Porosity - pore pressure relation
- Permeability - porosity relation

Provision is made for all practical boundary conditions. Furthermore, any face of any zone may be a boundary. Boundary condition options include:

- Impermeable, insulated
- Impermeable, prescribed heat flux
- Impermeable, prescribed temperature
- Prescribed mass flux, insulated
- Prescribed mass flux, prescribed heat flux
- Prescribed mass flux, prescribed temperature
- Prescribed pressure/heat content

In its present form QUAGMR is thus a very general tool for analyzing the transport of mass and heat in a quasi-active geothermal reservoir. It is, however, basically a testbed computer program; its flexibility and generality are desirable features for Phase II of this research effort which calls for coupling QUAGMR to a program which treats the full stress-strain field in the rock matrix and thereby to obtain a fully active reservoir simulator (see Section 3.3). Further details

of the evolving numerical procedures and program structure will be delayed until after the code development work is completed.

3.2 FINITE ELEMENT STRUCTURAL EQUILIBRIUM CODE

In order to model the effect of time-varying rock (matrix) stress on fluid flow in a geothermal reservoir, and also to monitor surface subsidence, a finite element solid equilibrium code, STAGR (STatic Analysis of Geothermal Reservoirs) has been developed. Like any such finite element code, it is basically a program for solving the problem of a loaded linear elastic continuum; however, materially nonlinear problems may be solved by iteration, using effective elastic moduli ("tangent" or "secant" moduli) in the elements [Desai and Abel, 1972]. Due to the very small matrix displacements expected in geothermal reservoir calculations, only material nonlinearity, and not geometric nonlinearity, has been included.

In addition to the usual features found in finite element continuum codes, STAGR can solve problems involving non-symmetric stress-strain relations (necessary for problems involving incremental loading of materials which undergo plastic deformation). This requires the use of a non-symmetric stiffness matrix.

The finite element technique for linear analysis of an elastic continuum, which forms the basis for the nonlinear treatment, proceeds in steps:

1. Discretization of the continuum. The volume of interest in the physical problem is divided into elements. In two dimensions, it is convenient to use triangles as the basic element; quadrilateral elements are formed from four triangles,

and through the technique of nodal condensation [Desai and Abel, 1972] the internal nodal degrees of freedom are removed. Hexahedral (brick) elements are used in three dimensions.

2. Selection of shape functions. The displacement field in the continuum is assumed to be of the form

$$\underline{u}(\underline{x}) = \sum_i \underline{u}_i \, N_i(\underline{x}) \tag{3.10}$$

where the summation is over all nodes i (which are corners of elements), the $\underline{u}_i$ are the nodal displacements, and $N_i(\underline{x})$ is the shape function associated with node i. The shape functions have the property that $N_i(\underline{x})$ is nonzero only in elements adjacent to node i, thus giving rise to the term "finite element"; this differs from a "global" approach such as a Fourier expansion, in which the $N_i(\underline{x})$ would in general be nonzero everywhere.

3. Calculation of element stiffness matrices. The principle of minimum potential energy [Desai and Abel, 1972] is applied to the continuum as the basic principle for determining the nodal displacements $\underline{u}_i$, which are the unknowns in the problem. In the case of a linear elastic continuum, the principle of minimum potential energy is equivalent to the differential equations of structural equilibrium. The analysis for materially nonlinear systems is built around the linear problem. As applied to each element of the continuum, the principle of minimum potential energy yields a linear relation

between the nodal displacement vector of the element, $\{q_e\}$, and the element nodal force vector $\{Q_e\}$:

$$[k_e]\ \{q_e\} = \{Q_e\} \tag{3.11}$$

where $[k_e]$ is called the element stiffness matrix.

4. Assembly of the global stiffness matrix. The element stiffness matrices are summed directly to form the global stiffness matrix $[K]$:

$$[K] = \sum_e [k_e] \tag{3.12}$$

where the sum is over all elements of the continuum. Also, the nodal force (load) vectors are added to form the global load vector R:

$$\{R\} = \sum_e \{Q_e\} \ . \tag{3.13}$$

5. Solution for the nodal displacements. The principle of minimum potential energy for the continuum is

$$[K]\ \{r\} = \{R\} \tag{3.14}$$

where r is the global nodal displacement vector. The solution of (3.14) is accomplished by Gauss elimination [Dahlquist and Bjorck, 1974]; the matrix $[K]$ is converted to upper triangular form, and the nodal displacements $\{r\}$ are solved for by back-substitution.

6. Computation of element strains and stresses. The nodal displacements $\{r\}$ are used to compute element strains, which are then used (through the element stress-strain relations) to compute element stresses. This completes the solution of the equilibrium configuration of the linear continuum.

In order to treat material nonlinearity, it is necessary to iterate, using effective elastic moduli in the elements. For this purpose, the initial stiffness matrix $[K_0]$ of the system (i.e., the stiffness matrix at the start of the problem) may be used. This saves the computational labor of recomputing $[K]$ at each iteration. The procedure is as follows:

An iteration is performed, with iteration index $i = 1, 2, \ldots,$ in which displacement increments Δr_i are computed by solving the linear equation system

$$[K_0] \{\Delta r_i\} = \{R_i\}$$

where the incremental load vector $\{R_i\}$ will be defined below. The iteration over i is continued to convergence, i.e., until, for example, the maximum absolute value of any component of $\{\Delta r_i\}$ is less than some prescribed tolerance. The net displacement after i iteration is

$$\{r_i\} = \sum_{j=1}^{i} \{\Delta r_j\}$$

The incremental load vector R_i is given by

$$\{R_i\} = \{R\} - \{R_{e,i-1}\}$$

where $\{R\}$ is the total system load vector, and $\{R_{e,i}\}$ is the load necessary to maintain the displacements $\{q_i\}$. $\{R_{e,i}\}$ is given by

$$\{R_{e,i}\} = \int_V [B]^T \{\sigma_i\} \, dV$$

where V is the reservoir volume, $\{\sigma_i\}$ is the vector of stress components, and $[B]^T$ is the transpose of the matrix $[B]$ which relates strains and displacements in the continuum.

The stress vector $\{\sigma_i\}$ is obtained from the constitutive relations for the system, which enable one to obtain the element stresses in terms of element strains, which are obtained from the displacements at iteration i, $\{q_i\}$.

3.3 INTEGRATION OF STRUCTURAL EQUILIBRIUM AND QUAGMR CODES

The QUAGMR code treats the problem of a quasi-active geothermal reservoir, i.e., one in which the state of total stress (rock stress plus fluid stress) is time-independent, so that the rock porosity depends only on fluid pressure. The coupling between the rock and fluid, in the fully active reservoir model, introduces the state of total stress as parameterizing the porosity-fluid pressure relation. In the fully active model, the fluid mass and energy conservation equations will be marched through discrete time steps, and at the end of each time step not only the finite difference analogs of the fluid conservation equations, but also the structural equilibrium equation will be satisfied.

The computational procedure for linking the fluid and structure phases is shown in Fig. 3.2. Each time step consists of an outer iteration loop, as indicated. Within this outer iteration, a fluid variable iteration is performed in which the state of total stress is assumed constant. At this point, the fluid variables and the rock thermal energy have been changed. These new variables are then fed into the

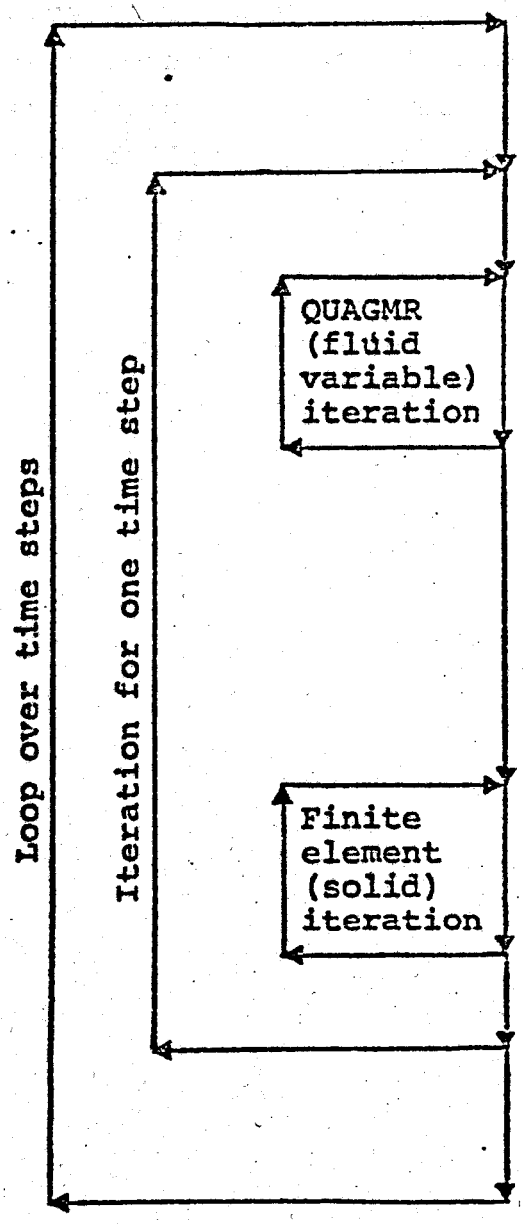

Figure 3.2. Computational procedure for coupling fluid and structure calculations.

constitutive relations for the stress-strain relation of the reservoir system, and the nonlinear structural equilibrium code is then iterated to convergence, yielding a new state of total stress. This sequence of fluid/rock iterations is itself iterated until complete convergence of all dependent variables is obtained; this constitutes one time step. Implementation of this computational procedure to develop a fully active reservoir simulator will be completed in Phase II.

IV. VERIFICATION OF THE FLUID-FLOW MODEL AND PRELIMINARY APPLICATIONS

An experimental effort is underway at Stanford University to obtain fundamental heat and mass transfer data (Kruger and Ramey [1974]; Arihara [1974]) on single and two-phase flow through porous media. These experimental data are ideal for verifying the quasi-active fluid flow model described in Section 3.1. The numerical simulator QUAGMR has been applied to study transport of mass and energy in linear bench-scale models. Comparison of theoretical predictions with experimental data shows excellent agreement (Section 4.1); it is, therefore, safe to conclude that the fluid flow model contains all the significant thermomechanical effects associated with multi-phase flow through porous media. The quasi-active fluid flow model has also been applied to perform preliminary two-dimensional production/injection calculations for a hypothetical hydrothermal reservoir; these calculations show that production with injection can lead to higher gross power output than production without injection (Section 4.2). In Section 4.3, we apply the rock response computer model of Section 3.2 to perform preliminary calculations of land-surface subsidence due to fluid production (and consequent reduction in pore pressure) from a hypothetical hydrothermal reservoir. The results indicate that fluid withdrawal (without reinjection) may lead to substantial surface deformations. Maximum horizontal displacements are calculated to be approximately one-fourth as large as maximum vertical displacements for the problem treated. The principal perturbation of the initial in situ stress field caused by the depletion of the reservoir is a reduction of the horizontal compressive stress component.

4.1 SIMULATION OF LINEAR BENCH-SCALE EXPERIMENTS

Researchers at Stanford University are conducting experimental studies on bench-scale linear flow models to test fundamental concepts for nonisothermal single-phase (liquid water) and boiling two-phase (water/water vapor) flow through porous media. A schematic of the experimental set-up is shown in Fig. 4.1a. The core holder (containing the test model) is provided with inlet and outlet pipes, and is held in an oven. In general, the oven temperature (T_∞) may be different from the core temperature; heat transfer to (or from) the core will generally take place from the brass plug ends and the sides of the core holder. The core rock in the experiments to be described below was a synthetic consolidated sandstone (sand - 80 percent, cement - 20 percent). Further details of the experimental set-up may be found in Kruger and Ramey [1974] and Arihara [1974].

Fluid flow through the core was numerically simulated as a one-dimensional problem (Fig. 4.1b). The core length ($\sim$ 60 cm) is divided into 10 zones of 6 cm each. Heat gain (or loss) through the sides and the ends is represented by volumetric source (sink) terms. Heat source from the sides is added to each cell, and is given by

$$\dot{q}_s = h_s\ (T_\infty - T)\ \text{ergs/sec cm}^3$$

where h_s is an empirically determined constant. Heat gain (or loss) from the left end is added only to the cell adjoining the left boundary:

$$\dot{q}_e = h_e\ (T_\infty - T)\ \text{ergs/sec cm}^3$$

where h_e is an empirically determined constant. No experimental data are available for heat flux through the brass plugs. The value of h_e must, therefore, be estimated from

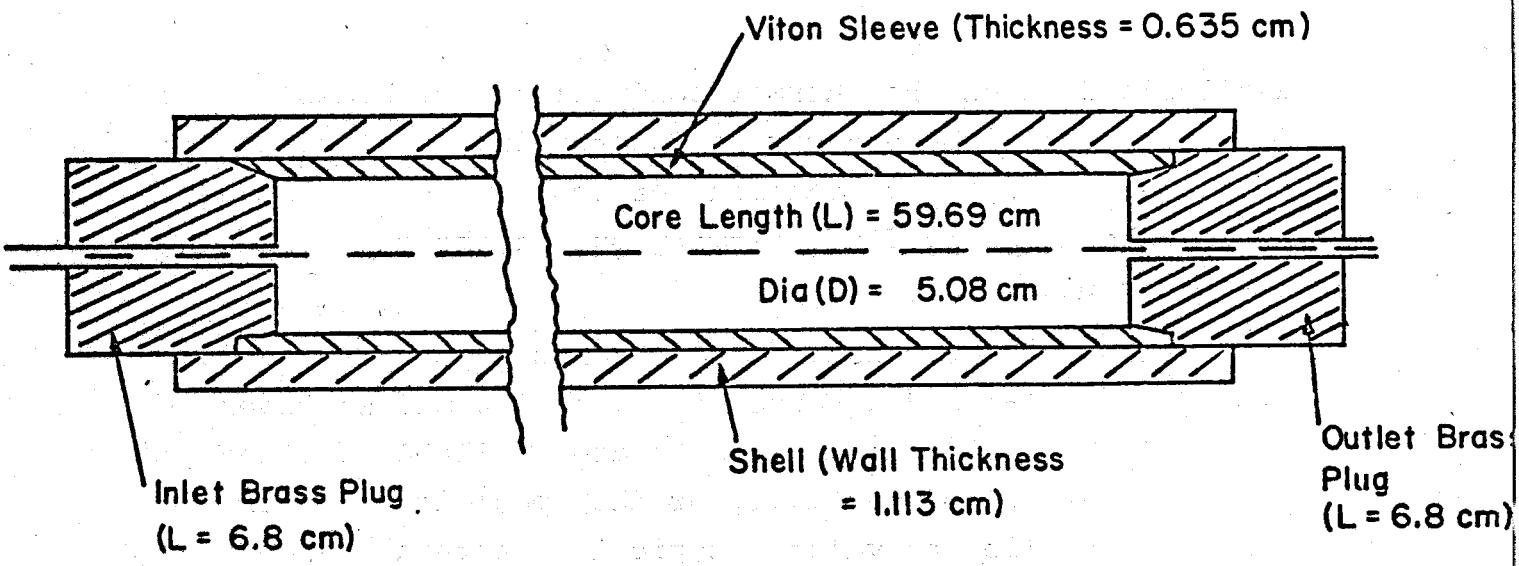

Figure 4.1a. Schematic of experimental set-up.

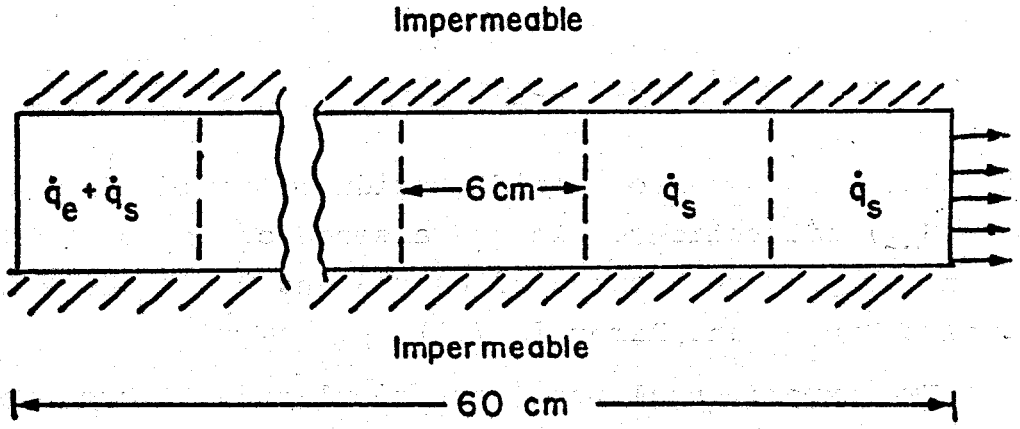

Figure 4.1b. One-dimensional numerical model. Convective heat fluxes from the left end and the sdies are represented by volumetric source terms (q_e and q_s). The left boundary is either impermeable or has specified inflow conditions; outflow conditions are prescribed at the right boundary.

available data on the thermal conductivity of brass. Heat flux from the right end may be ignored in the first approximation since any heat addition (or loss) would be largely advected out by the fluid flowing out of the core through the brass plug.

The synthetic sandstone core has a porosity of 36 percent ($\phi_0 = 0.36$) and a permeability of 100 millidarcies ($k = 100$ md $= 10^{-9}$ cm^2). No data are available for the grain density, thermal conductivity or the specific heat for the core. The following values, typical of natural sandstones, will be assumed for these material properties:

$$C_{Vs} = 10^7 \text{ ergs/gm°C}$$

$$\rho_s = 2.65 \text{ gm/cm}^3$$

$$\kappa_s = 2.1\times10^5 \text{ ergs/sec cm°C}$$

It is also necessary to specify residual liquid ($S_{\ell r}$) and vapor (S_{vr}) saturations. In the absence of any other data, $S_{\ell r}$ and S_{vr} were assumed to be 0.3 and 0.05, respectively (see also Kruger and Ramey [1974]).

Two experimental runs were simulated. These are (1) injection of cold water into a core containing hot water and (2) production of hot water and steam from a system containing pressurized water. In the first simulation, it is necessary to specify the mass flow rate ($= (4.4\times10^{-3} - 1.6\times10^{-7}\,t)$ gm/sec, t is in sec), and the injection temperature ($t < 7$ min, $T_{inlet} = 67.7$°C; 7 min $\leq t \leq$ 15 min, $T_{inlet} = (67.7 - 1.3125\,(t-7))$°C, t is in min; $t >$ 15 min, $T_{inlet} = 57.2$°C) at the left boundary, initial temperature of core containing hot water (120.6°C), oven temperature (assumed to be 120.6°C), pressure at the right boundary ($= (14 - 3.704\times10^{-4}\,t)$ bars, t is in sec), h_s ($= 1.16\times10^4$), and h_e ($=0$). Specification

of the inlet temperature automatically takes into account the heat flow into the core from the left end, and hence h_e is assumed to be zero for the purposes of numerical simulation. For the second simulation, the left boundary is impermeable (no inflow into core); initial pressure and temperature of the pressurized water are 18.37 bars and a linear variation between 183°C (at the right end) and 192°C at the left end (see Fig. 4.4); the oven temperature is 198.9°C; the pressure history imposed at the right boundary is shown as an insert in Fig. 4.3. The following values were assumed for h_e and h_s:

$$h_e = 5.42\times10^5,\ h_s = 1.78\times10^4.$$

The value of h_e represents only an estimate and may be in substantial error.

As remarked in the preceding, the fluid flow in the first experiment is entirely single phase. Calculated temperatures profiles at various times along with experimental data are shown in Fig. 4.2. In general, good correlation is observed. Slight differences between the theoretical results and experimental data observed in Fig. 4.2 may be due to uncertainties in input data (e.g., bath temperature, thermodynamic properties of core, and pressure conditions at the right boundary) and relatively crude zoning (zone size $\sim$ 6 cm) employed in the numerical simulation.

The second experiment represents a more severe test of the theoretical model insofar as the fluid flow through the core is two-phase (water/steam). Calculated pressure and temperature profiles along with experimental measurements are shown in Figs. 4.3 and 4.4, respectively. Once again, experimental data are seen to be in good agreement with theoretical results. This agreement is all the more gratifying when we consider the uncertainties in input data for rock

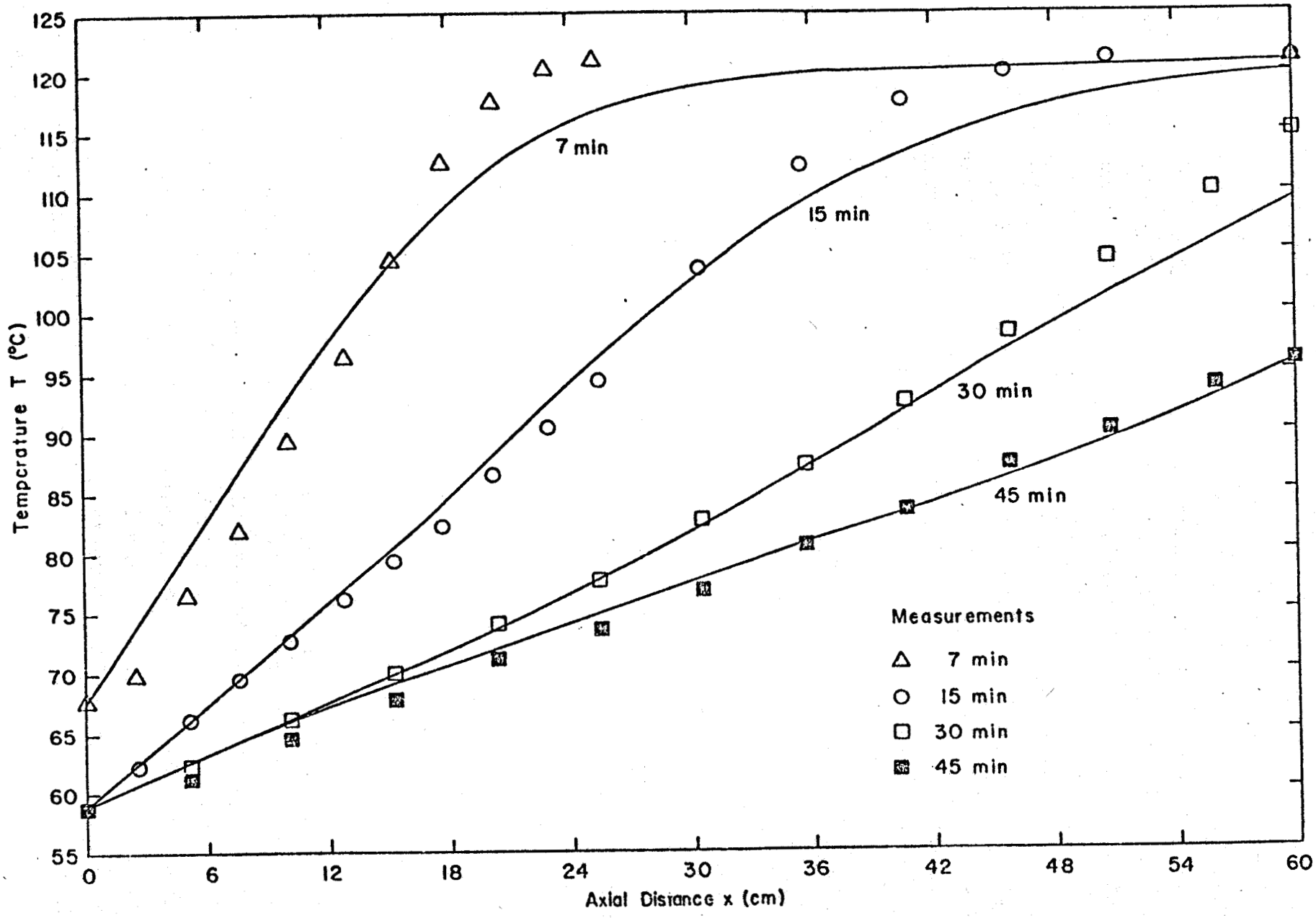

Figure 4.2. Comparison of calculated temperature profiles (solid lines) with experimental data (single phase flow) of Arihara [1974].

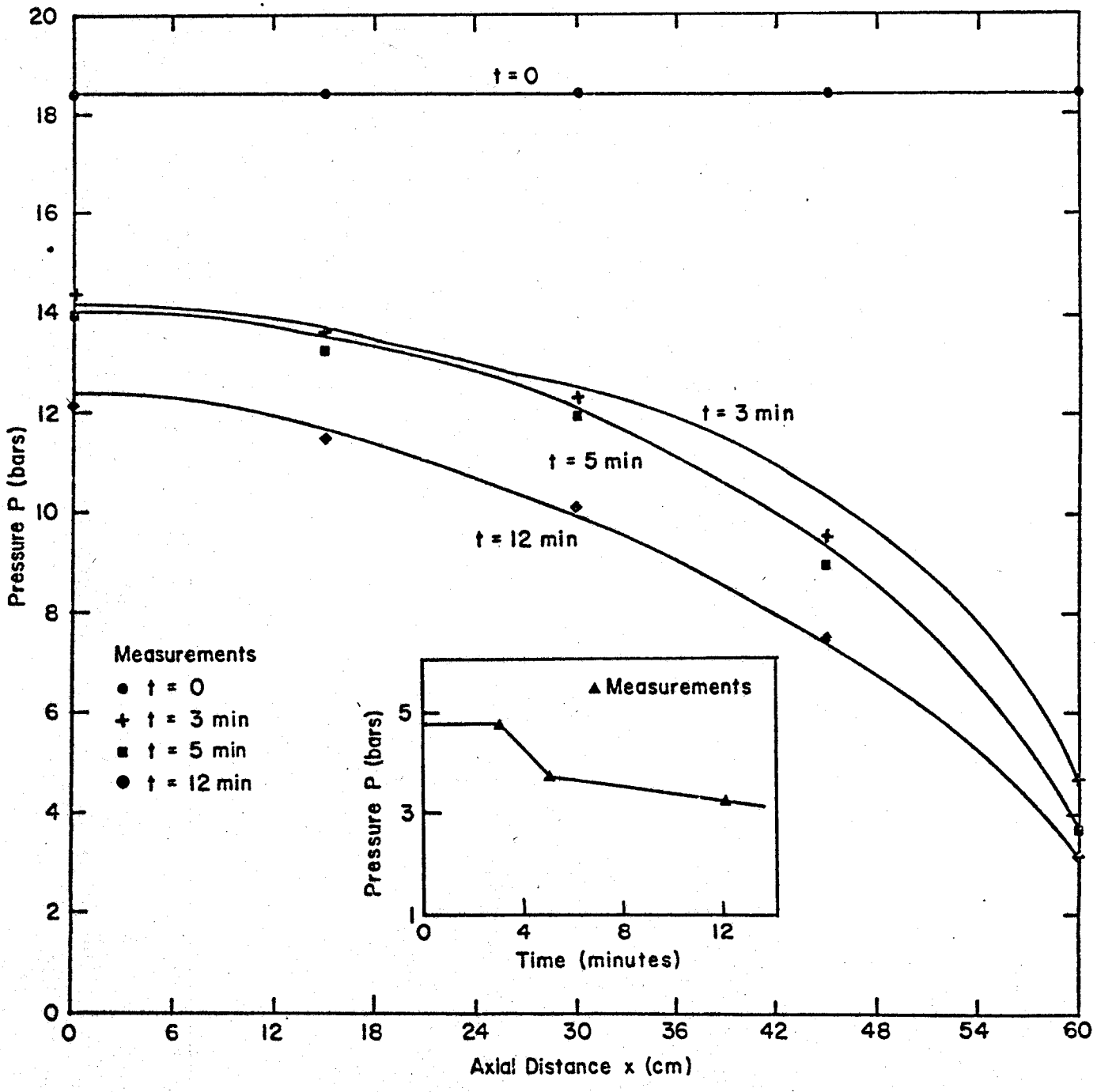

Figure 4.3. Comparison of calculated pressure profiles (solid lines) with experimental data (two-phase flow) of Kruger and Ramey [1974]. Insert shows the simulated pressure history on the right boundary.

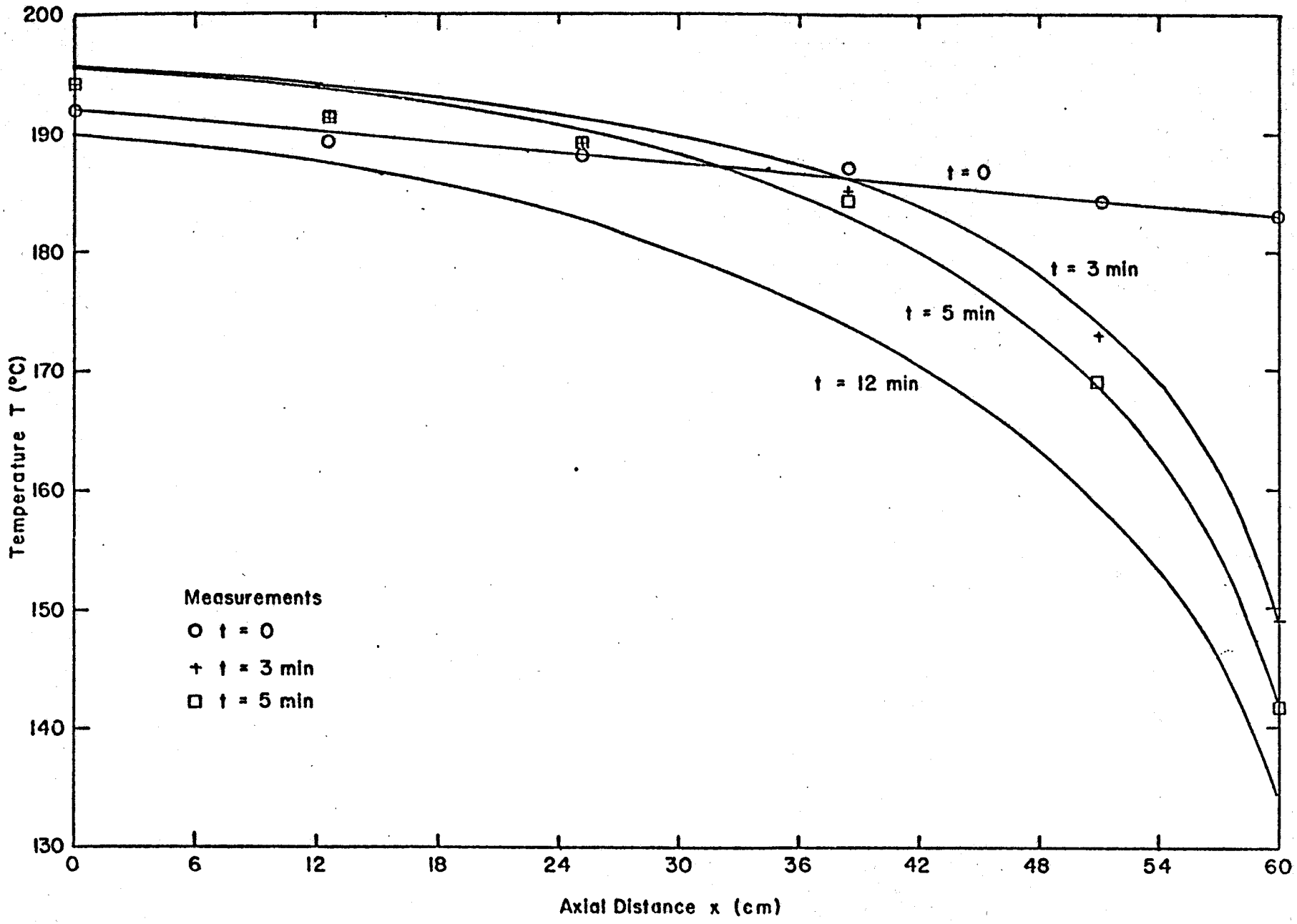

Figure 4.4. Comparison of calculated temperature profiles (solid lines) with experimental data (two-phase flow) of Kruger and Ramey [1974].

properties and vapor pressure for water. (Note that the vapor pressure data utilized in the tabular equation-of-state for water were measured for flat surface interfaces. If the steam-water interface is a curved surface, as might happen in porous media, then vapor pressure may be significantly lowered (Kruger and Ramey [1974]). No experimental data are available for vapor saturation; calculated vapor saturation profiles are shown in Fig. 4.5. It is seen from Fig. 4.5 that boiling first occurs at the ends of the core (initial boiling at the left end is due to the higher initial temperature at this end), and then spreads to the middle of the core.

4.2 2D RESERVOIR CALCULATIONS

In this section, some preliminary results for production from and injection into a hypothetical bounded hydrothermal reservoir will be discussed. The reservoir is assumed to be a right circular cylinder (horizontal cross-sections of the reservoir are circles). A two-dimensional areal representation of the reservoir along with the numerical grid is shown in Fig. 4.6. The reservoir diameter is 3.3 km and its vertical thickness is 100 m. Production takes place from a central vertical crack of length 900 m, and fluid reinjection is into two similar cracks located at the reservoir periphery, as shown in the figure. The reservoir initially contains pressurized water at P = 200 bars and T = 300°C. The reservoir rock is assumed to be a "typical sandstone" with the following properties:

ρ_s (grain density) = 2.65 gm/cm

ϕ (porosity) = ϕ_0 = 0.2

κ_s (thermal conductivity) = 2.1×10^5 ergs/sec cm°C

k (permeability) = k_0 = 200 md = 2×10^{-9} cm^2

C_{Vs} (specific heat) = 10^7 ergs/gm°C

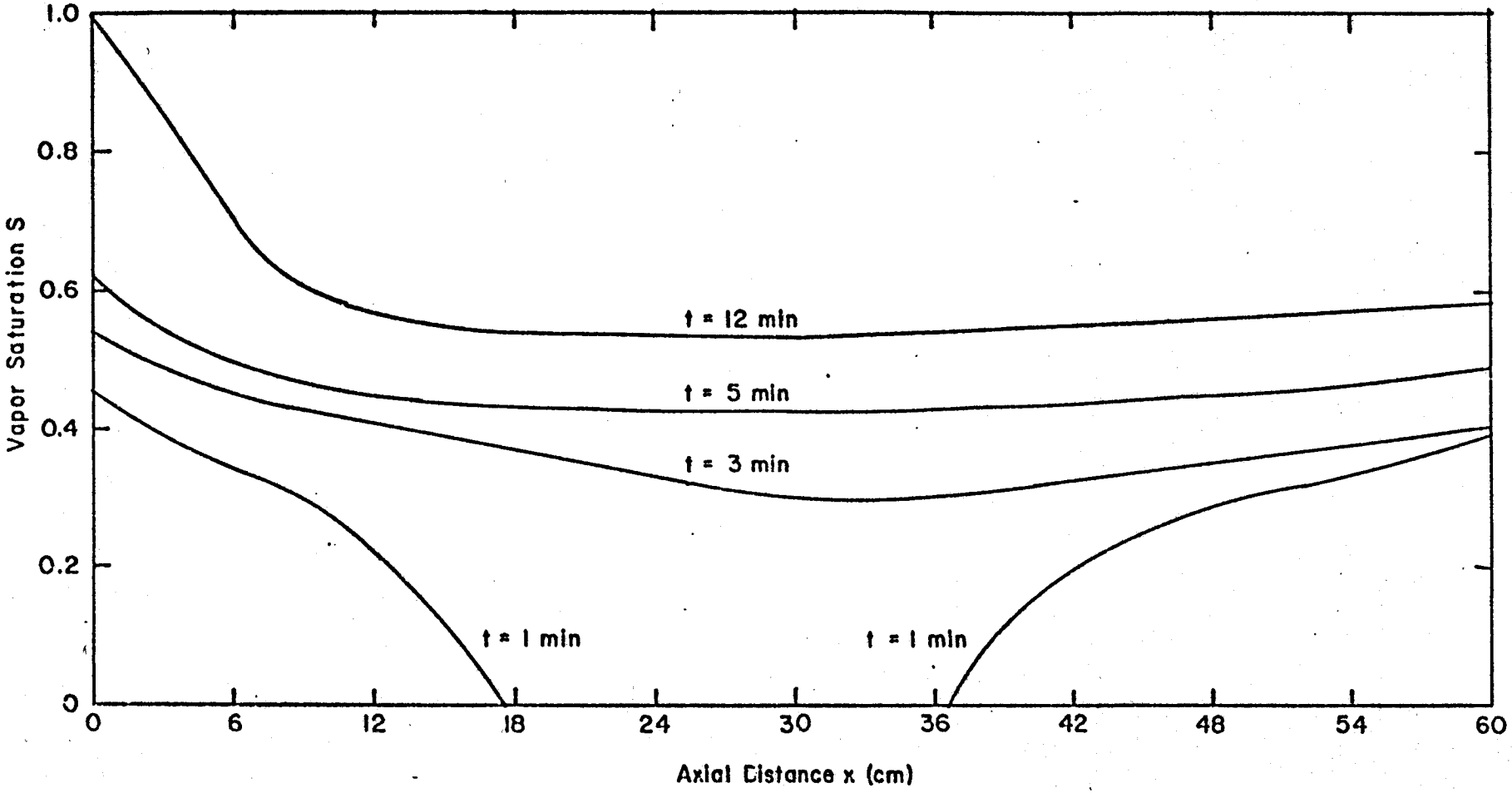

Figure 4.5. Vapor saturation profiles.

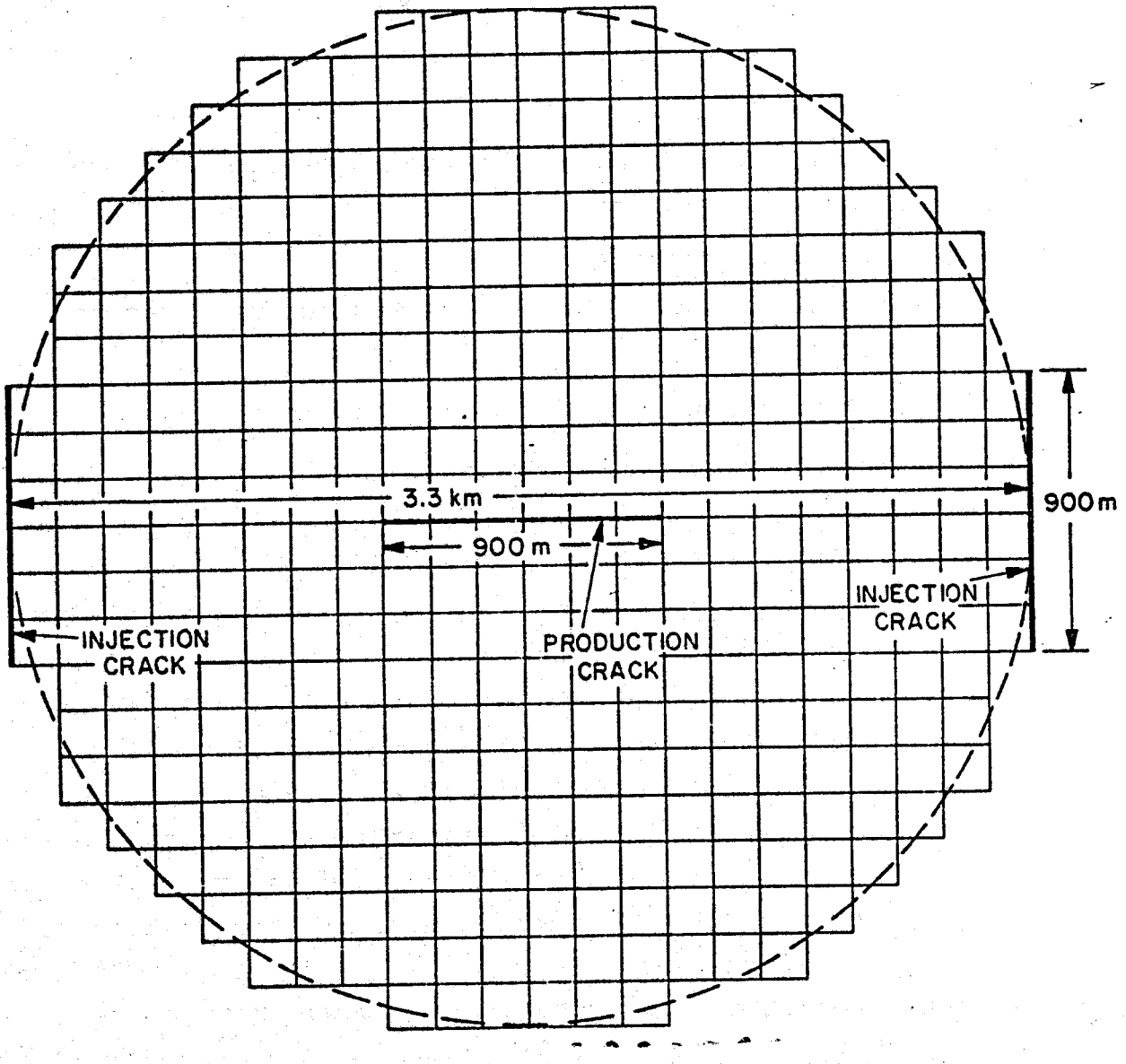

Figure 4.6. A cross-section of the hypothetical bounded hydrothermal reservoir. Production from or injection into the reservoir is allowed through production (injection) crack(s). The circular reservoir cross-section is approximated by a square mesh (384 zones; $\Delta x = \Delta y = 150$ m). No heat or mass flux is allowed across reservoir boundaries.

$S_{\ell r} = 0.3$

$S_{vr} = 0.05.$

Note that at T = 300°C, the saturation pressure is approximately 86 bars. Production at P < 86 bars will, therefore, result in in situ flashing.

A series of four calculations was run with the following production and injection conditions:

1. Production at P = 100 bars, no injection.
2. Production at P = 50 bars, no injection.
3. Production at P = 50 bars, injection at P = 200 bars and T = 100°C.
4. Production at P = 100 bars, injection at P = 200 bars and T = 100°C.

Fluid flow for the first and fourth cases is single phase; the second and third cases involve two-phase flow. Typical pressure and temperature contours at t = 1 year (third case) are shown in Figs. 4.7 and 4.8, respectively. It can be seen from Fig. 4.8 that at t = 1 year, the cold injected water is beginning to invade the production region; continuation of production for times much greater than t = 1 year would lead to drastic reductions in gross thermal power output.

A quantity of great interest in geothermal power production is the gross thermal power output; Fig. 4.9 shows the gross thermal power output history as a function of various production strategies (Cases 1-4). Production with injection (Cases 3 and 4) leads to higher gross output than production without injection (Cases 1 and 2). Note that injection helps to maintain the reservoir pressure (and hence fluid production rate). It should be emphasized here that the above calculations have only a qualitative significance in view of the various assumptions made for the reservoir geometry and rock properties.

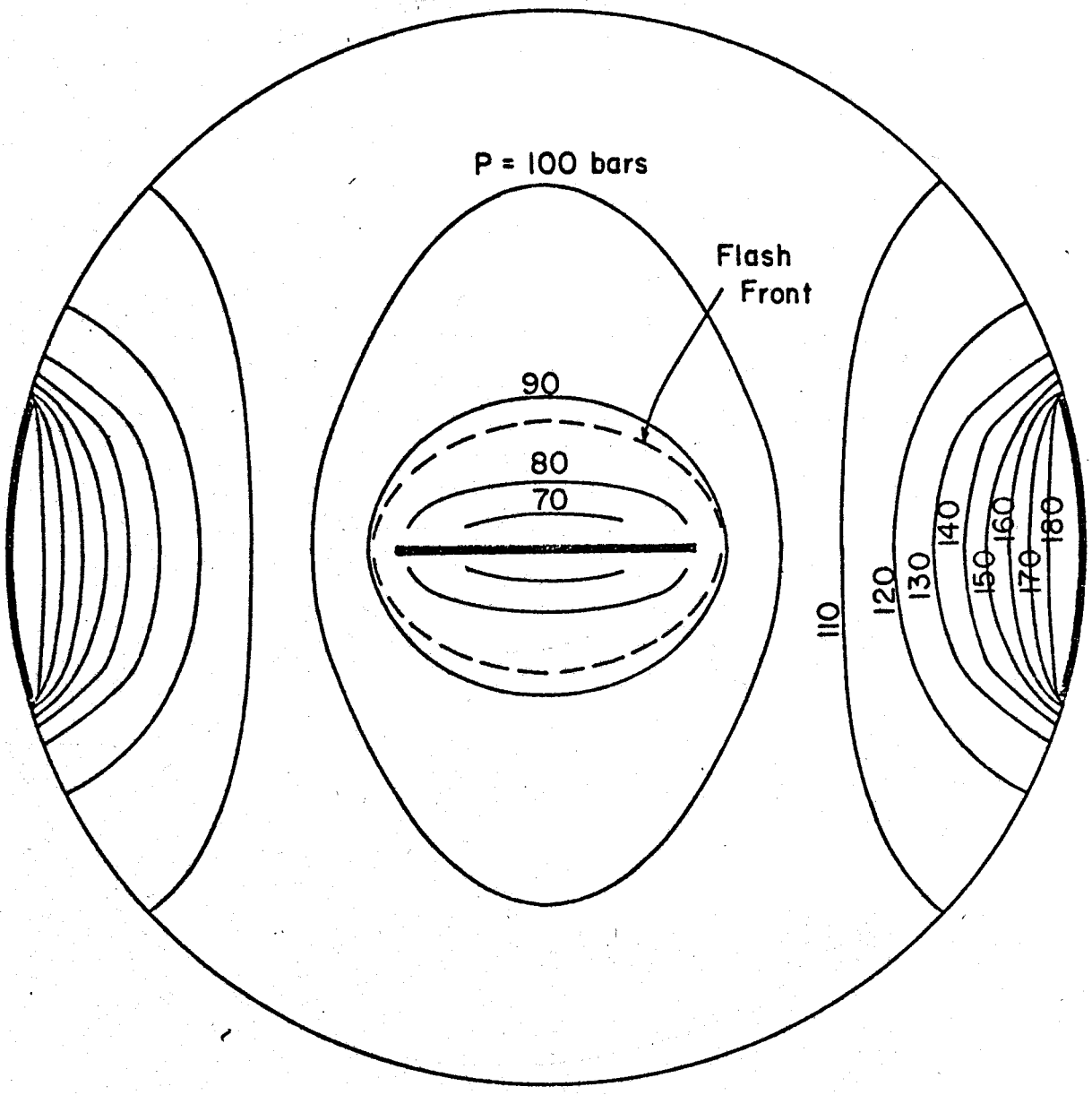

Figure 4.7. Pressure contours at t = 1 year (production at P = 50 bars, and injection at P = 200 bars and T = 100°C). The flash front is shown as a dotted line.

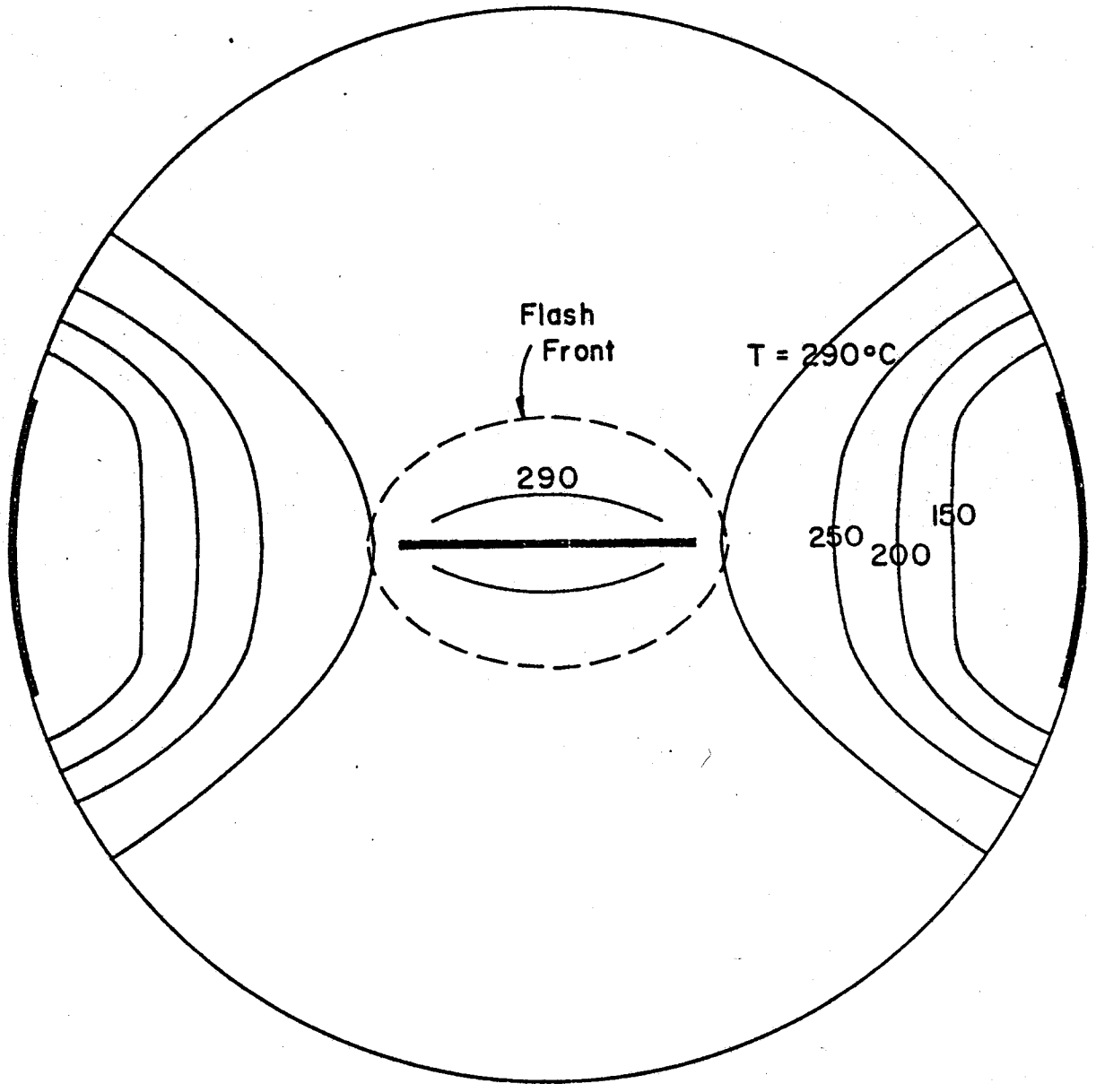

Figure 4.8. Temperature contours at t = 1 year (production at P = 50 bars, and injection at P = 200 bars and T = 100°C). The flash front is shown as a dotted line.

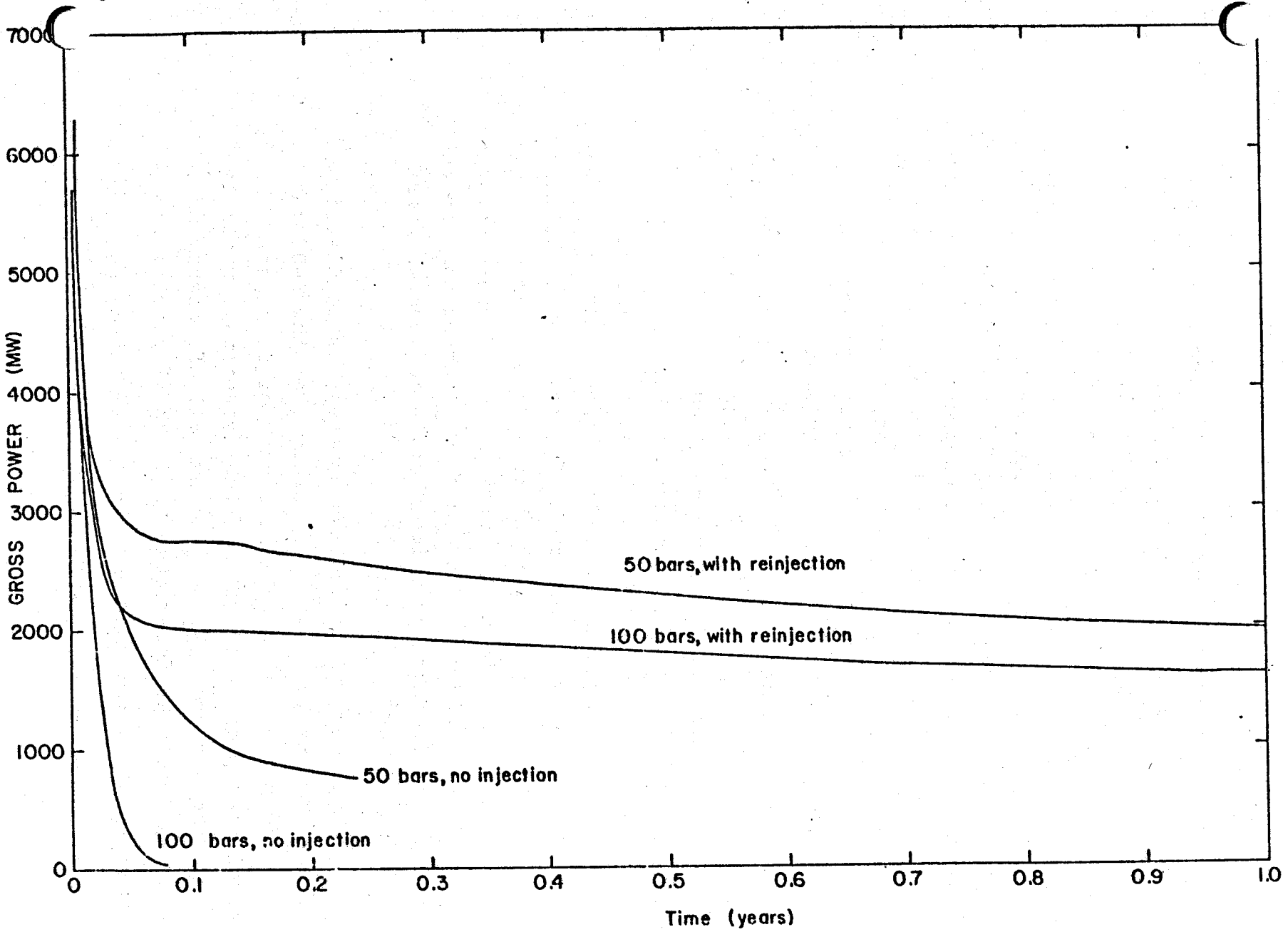

Figure 4.9. Gross power output (thermal) history for various production strategies.

4.3 2D SUBSIDENCE CALCULATIONS

In this section, the STAGR equilibrium code is used to perform 2D calculations of the rock response to production of a geothermal reservoir. As will be seen, the reservoir is entirely hypothetical; it is intended to represent, in a very crude way, a liquid-dominated convective hydrothermal system in a sedimentary rift trough such as the Imperial-Mexicali basin. It must be emphasized, however, that the results are only qualitative since rock properties were simply estimated, no faulting was permitted, no reinjection was considered, no natural recharge was allowed, the reservoir geometry was highly idealized, and the pore-pressure effects of production were treated in a very crude way.

The hypothetical geothermal basin was assumed to be 100 km in length. Impermeable cap rock occupies the uppermost 1 km of depth; permeable water-filled sandstone extends to 5 km depth; below that is impermeable basement rock. A cross section of the reservoir (with vertical dimensions exaggerated) is shown in Fig. 4.10; the long (100 km) dimension of the system is normal to the figure. As can be seen, the average width of the reservoir zone (from 1 km to 5 km in depth) is 50 km so that the surface area of the production region is 50 km × 100 km = 5000 km^2. The temperature in the sandstone layer is taken as uniform at 300°c, and the pore pressure is initially hydrostatic.

The hypothetical production strategy is to distribute 2500 production wells roughly uniformly over the 5000 km^2 area, and to produce each well at a rate of 50 kg/sec. Thus, the total mass production rate of the system as a whole is 1.25×10^5 kg/sec and, assuming an overall efficiency of 5 percent, the field produces about 5000 MW of electricity.

Since a coupled (QUAGMR/STAGR) code is not yet available, the pore-pressure history during the producing life-

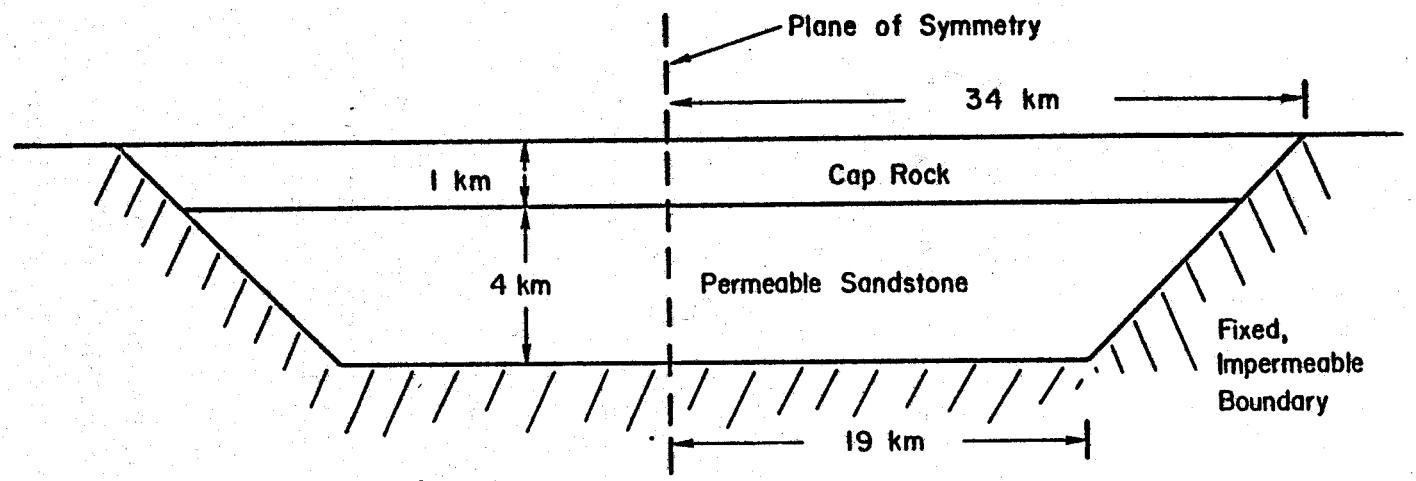

Figure 4.10. Vertical cross-section of hypothetical geothermal reservoir (vertical dimensions exaggerated 2.5 times).

time of the system was estimated in the following crude fashion for the purpose of the present calculation. The linearized single-phase governing equation for flow in the reservoir in the horizontal plane may be written:

$$\frac{\partial P}{\partial t} = \left(\frac{kA}{\mu\phi}\right) \nabla^2 P = \eta \nabla^2 P \qquad (4.1)$$

where

P = pore pressure

k = permeability

A = bulk modulus of the fluid

μ = fluid viscosity

ϕ = porosity

At 300°C, the bulk modulus of water is 5.71 kilobars and its viscosity is 9.55×10^{-4} poise. We will assume average values for porosity and permeability in the reservoir rock to be 0.15 and 100 millidarcies, respectively. Thus, the value of η is:

$$\eta = 3.986 \times 10^4 \text{ cm}^2/\text{sec} = 125.7 \text{ km}^2/\text{year}$$

Now, it may easily be shown that solution of Eq. (4.1) subject to time-dependent boundary conditions will reach steady state within about 1 percent by a time:

$$\tau = 2L^2/\eta$$

where L is a spatial dimension of the problem. In the present case, L is the average well spacing, or 1.414 km, so that steady state will be reached by a time:

$$\tau = 0.0318 \text{ year} = 11.6 \text{ days}$$

This means that on a time scale of years, the entire production region may be regarded as being produced uniformly.

The total volume of the reservoir rock region is 4 km × 50 km × 100 km = 20,000 km^3. With an average porosity of 15 percent, the total pore volume is 3000 km^3, so that the fluid mass in the system is initially about 3×10^{12} metric tons. As mentioned above, the initial production rate for the system as a whole is 125 metric tons/second, so that the density of the fluid in the reservoir changes at an initial rate given by:

$$\rho(g/cm^3) = \rho_0 - 1.314 \times 10^{-3} \times t$$

where t is in years. With a bulk modulus of 5.71 kilobars, this means that the pore pressure distribution in the reservoir, given initially by hydrostatic:

$$P\ (z,\ t = 0) = (100\ z)\ \text{bars}$$

(where z = depth below ground surface in km) declines at each point in the reservoir by 7.5 bars/year.

This pressure decline cannot continue indefinitely, however. At t = 1.867 years, the fluid at the top of the reservoir layer (z = 1 km) will have been reduced in pressure from its initial value of 100 bars to 86 bars. Now, 86 bars is the vapor pressure of water at 300°C. This means that at 1.867 years, a flash front will form at the top of the reservoir and begin moving downward through the system. The flash front will move downward at 0.075 kilometers per year. Above the flash front, the pressure will remain at 86 bars, the pressure of liquid water in equilibrium with water vapor at T = 300°C. At t = 55.2 years, the flash front will reach the basement rock. Thereafter, the system will be single phase and will be depleted rapidly.

The pore pressure history can thus be summarized as:

$$P(z,t) = \text{MAX}\ (86,\ [100z - 7.5\ t])\ \text{bars} \qquad (4.2)$$

for z ($\geq$ 1 km) in km and t in years

The cap rock is assumed to be linear elastic, with

E = Young's modulus = 60 kbar

ν = Poisson's ratio = 0.3

ρ = density = 2.2 gm/cm^3

so that the shear modulus is G = 23.08 kb. This value for G is also assumed for the reservoir rock. The reservoir grain density is 2.65 gm/cm^3.

The porosity-pressure relation for the sandstone is given by Eqs. (2.24) and (2.25); parameter values used in this calculation are

ϕ_0 = 0.15

K = 50 kb

K_s = 300 kb

The structural equilibrium equation, Eq. (2.6), was solved on the STAGR code for the system at times 0, 10, 20, 40 and 55.2 years, using the fluid pressure given in Eq. (4.2). Due to the symmetry of the system, the calculations were performed for one-half of the cross-section, with a vertical slip line boundary condition at the plane of symmetry.

The reservoir and cap rock regions are approximated by a rectangular mesh with ΔX = 1 km and ΔY = 1/3 km (see Fig. 4.11). The vertical (Y-ordinate) scale in Figs. 4.11 - 4.20 has been magnified by a factor of 6.8 for visual purposes. The initial state of rock/fluid mixture stress ($\sigma_i = -[(1-\phi)P_s + \phi P] + S_{ii}$, i = x,y; $\sigma_{xy} = S_{xy}$, etc.) is shown in Figs. 4.12 - 4.14. This initial state corresponds to loading the system with the initial (hydrostatic) pore pressure distribution discussed above, and with gravity.

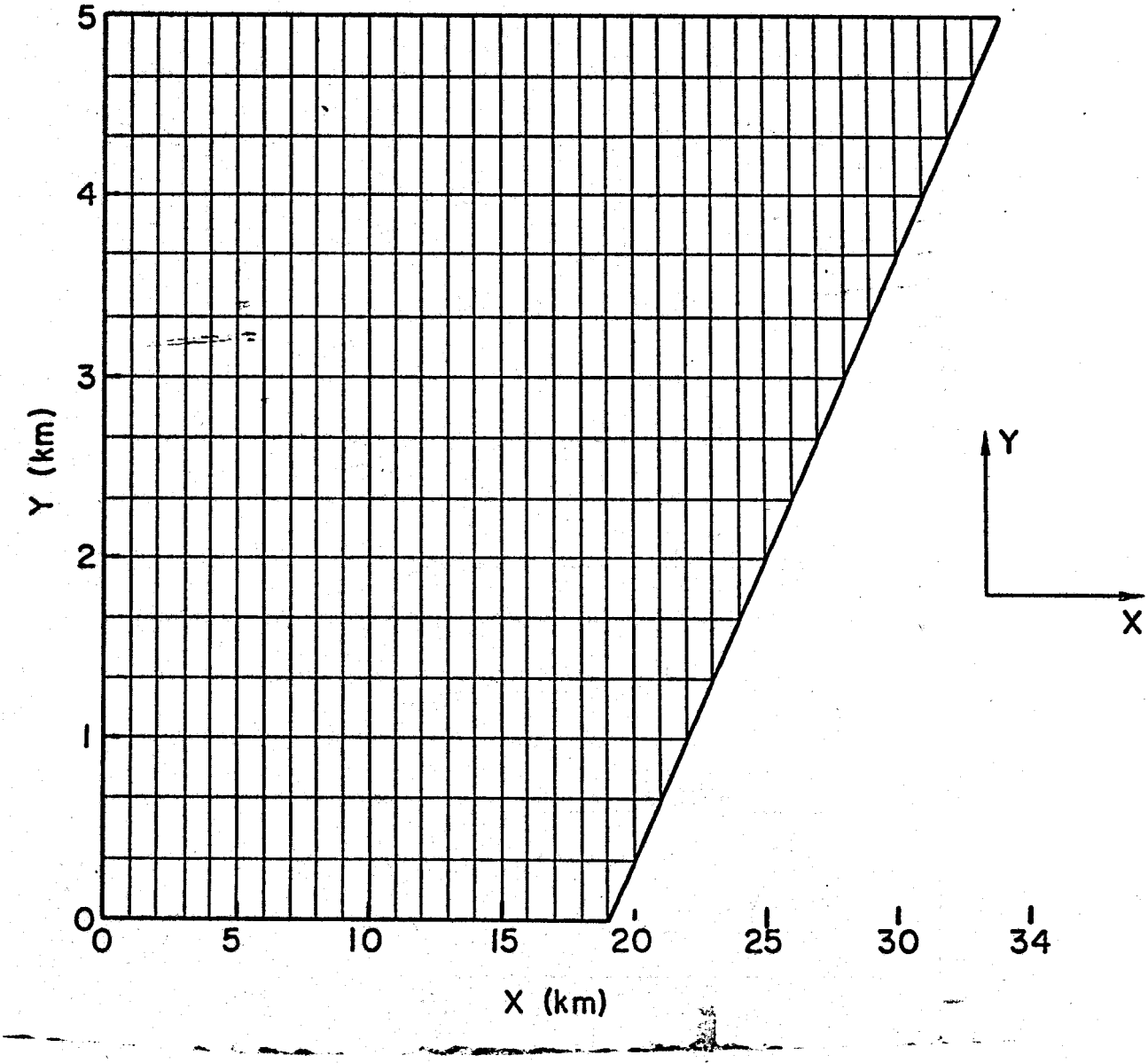

Figure 4.11. Computational grid (vertical scale has been magnified 6.8 times).

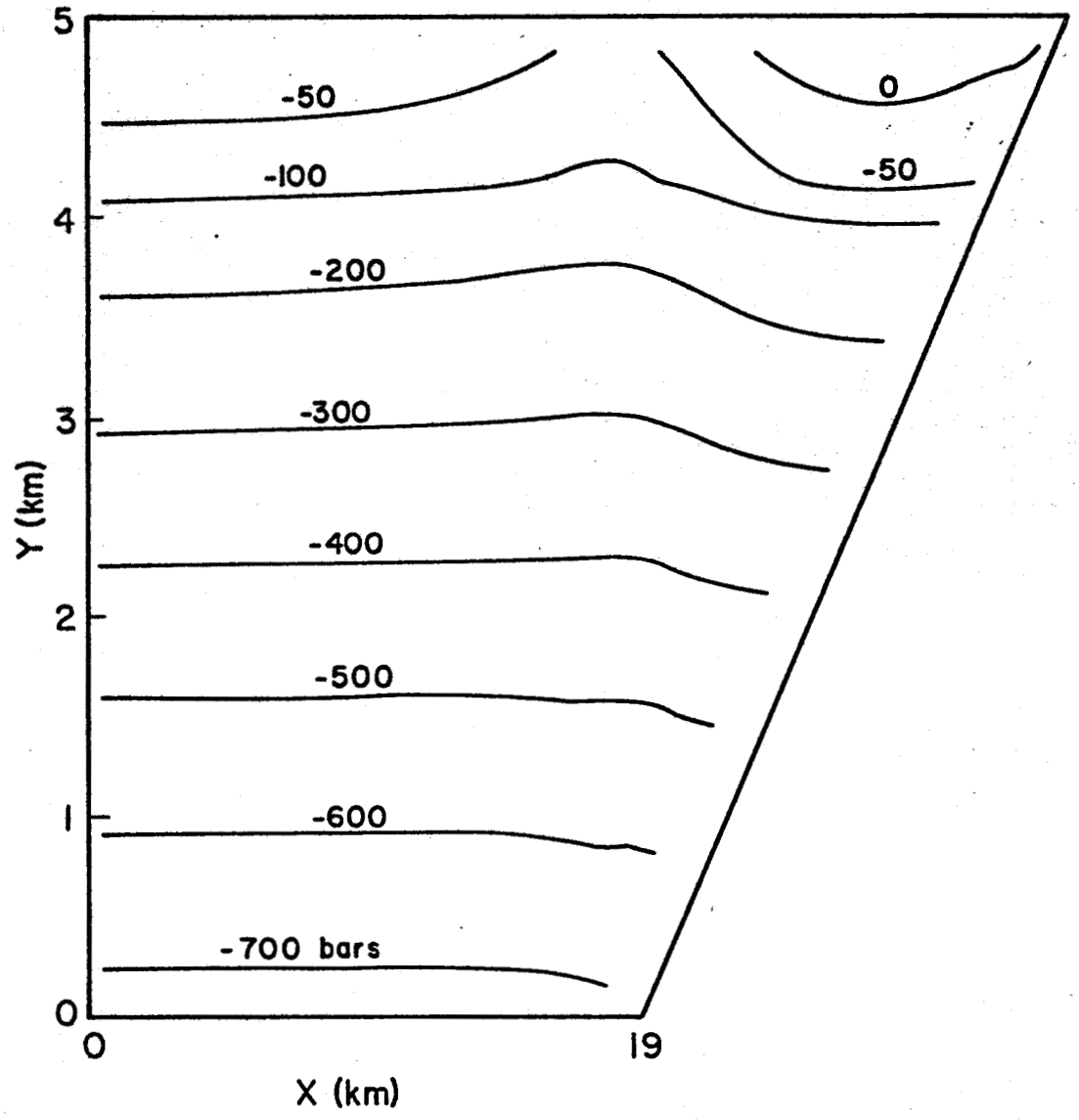

Figure 4.12. σ_x (horizontal stress) contours at t = 0 years.

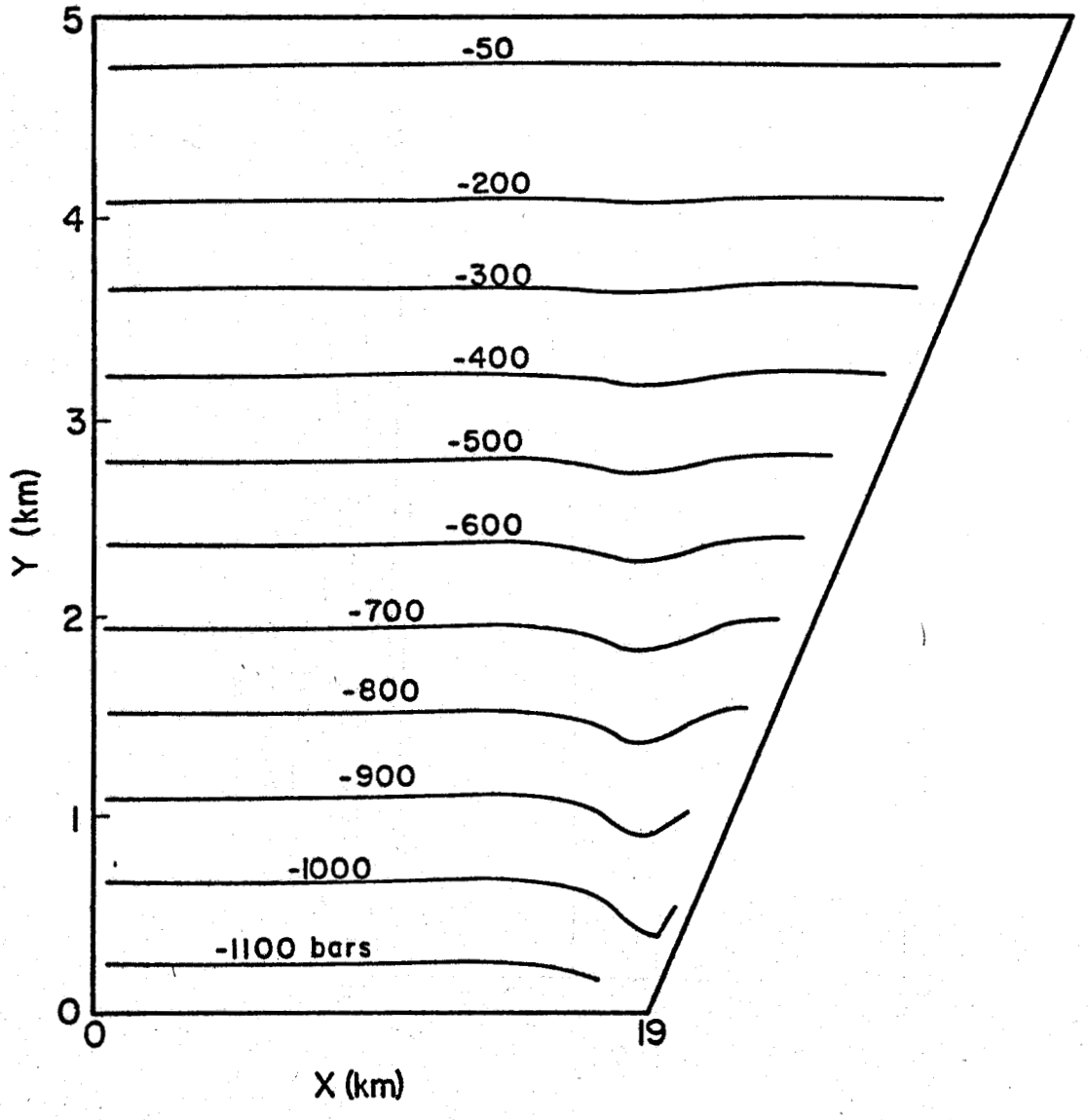

Figure 4.13. σ_y (vertical stress) contours at t = 0 years.

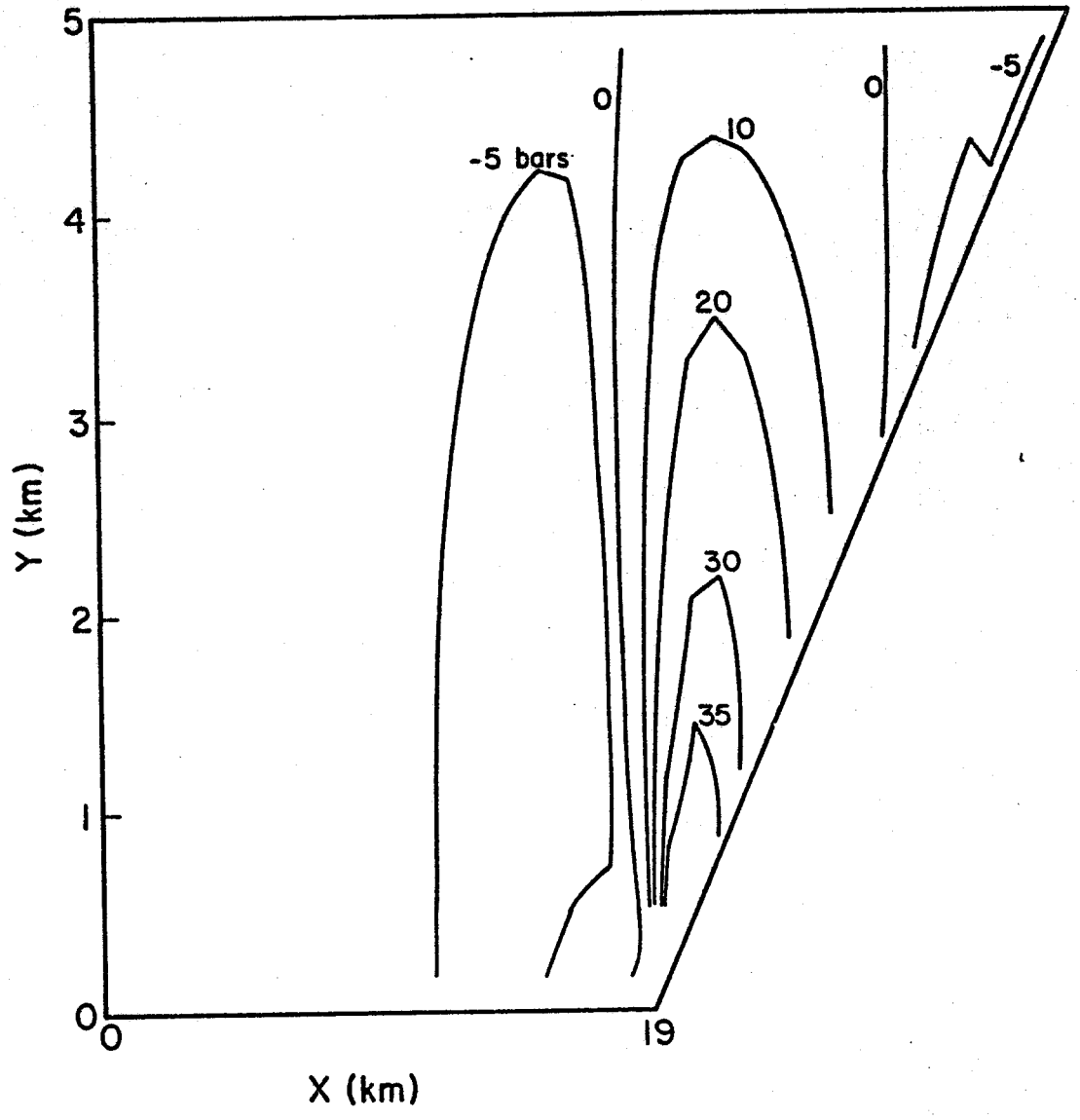

Figure 4.14. σ_{xy} (shear stress) contours at t = 0 years.

Both σ_x and σ_y are compressive, and are much greater than σ_{xy} ($|\sigma_x|$ and $|\sigma_y| >> |\sigma_{xy}|$). The latter observation implies that initially (t = 0), the principal stress directions are almost coincident with the x (horizontal) and y (vertical) directions. Changes induced in σ_x, σ_y, σ_{xy} by the production of reservoir fluids over 55.2 years are shown in Figs. 4.15, 4.16 and 4.17, respectively. We note that both MAX$|\Delta\sigma_y|$ ($\sim$ 24 bars) and MAX$|\Delta\sigma_{xy}|$ ($\sim$ 16 bars) are much smaller than MAX$|\Delta\sigma_x|$ ($\sim$ 180 bars). Thus, as a result of fluid production, σ_x becomes much less compressive whereas σ_y is essentially unaltered. This has interesting implications for reservoir stability. Large reductions in the magnitude of σ_x (such as computed above) without corresponding reductions in σ_y can lead to rock failure and growth of normal faults. Surface manifestation of these phenomena may be localized reservoir slumping, and increased seismic activity. For purposes of the present analysis, however, rock failure was not considered.

Rock displacements are shown in Figs. 4.18 - 4.20. Figure 4.18 is a vector plot of displacements; vectors are mainly directed downwards (indicating subsidence) and slightly towards the centerline (indicating horizontal motion). Deviations from the vertical are almost invisible in the figure, however, owing to the vertical scale exaggeration. Vertical displacement contours (Fig. 4.20) show that the central portion of the reservoir subsides almost uniformly ($\sim$ 8.5 m). Elsewhere, the vertical motion is accompanied by significant horizontal movement ($\sim$ 2 m, see Fig. 4.19). Experience from oilfields (e.g., Wilmington oil field in Los Angeles basin) indicates that horizontal motion may cause even more severe damage to surface installations (e.g., roads, bridges and buildings) than that caused by vertical subsidence. Thus, in order to assess the possible environmental impact of fluid production from geothermal reservoirs, it is necessary to take

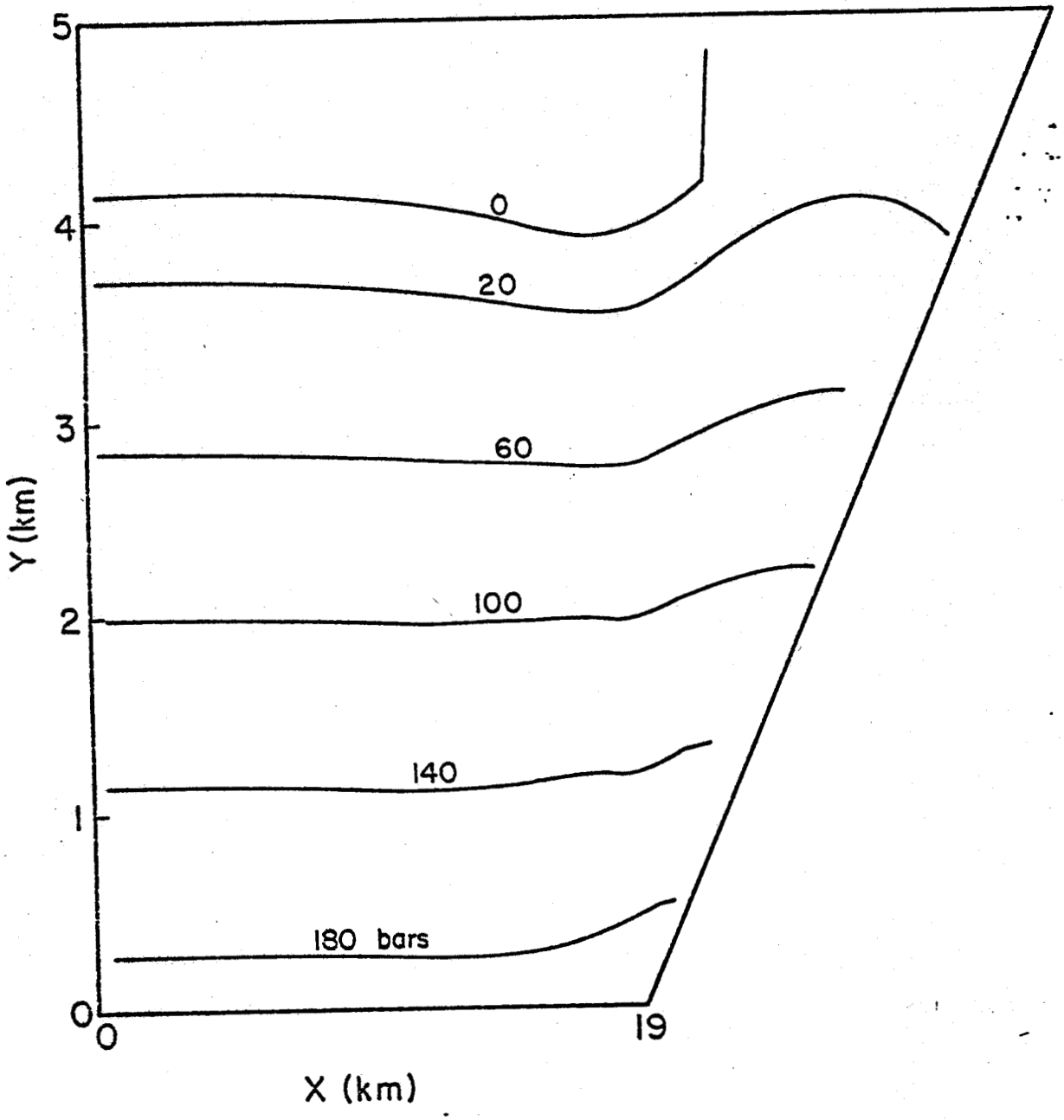

Figure 4.15. $\Delta\sigma_x$ [$=\sigma_x$ (t = 55.2 years) - σ_x (t = 0 years)] contours

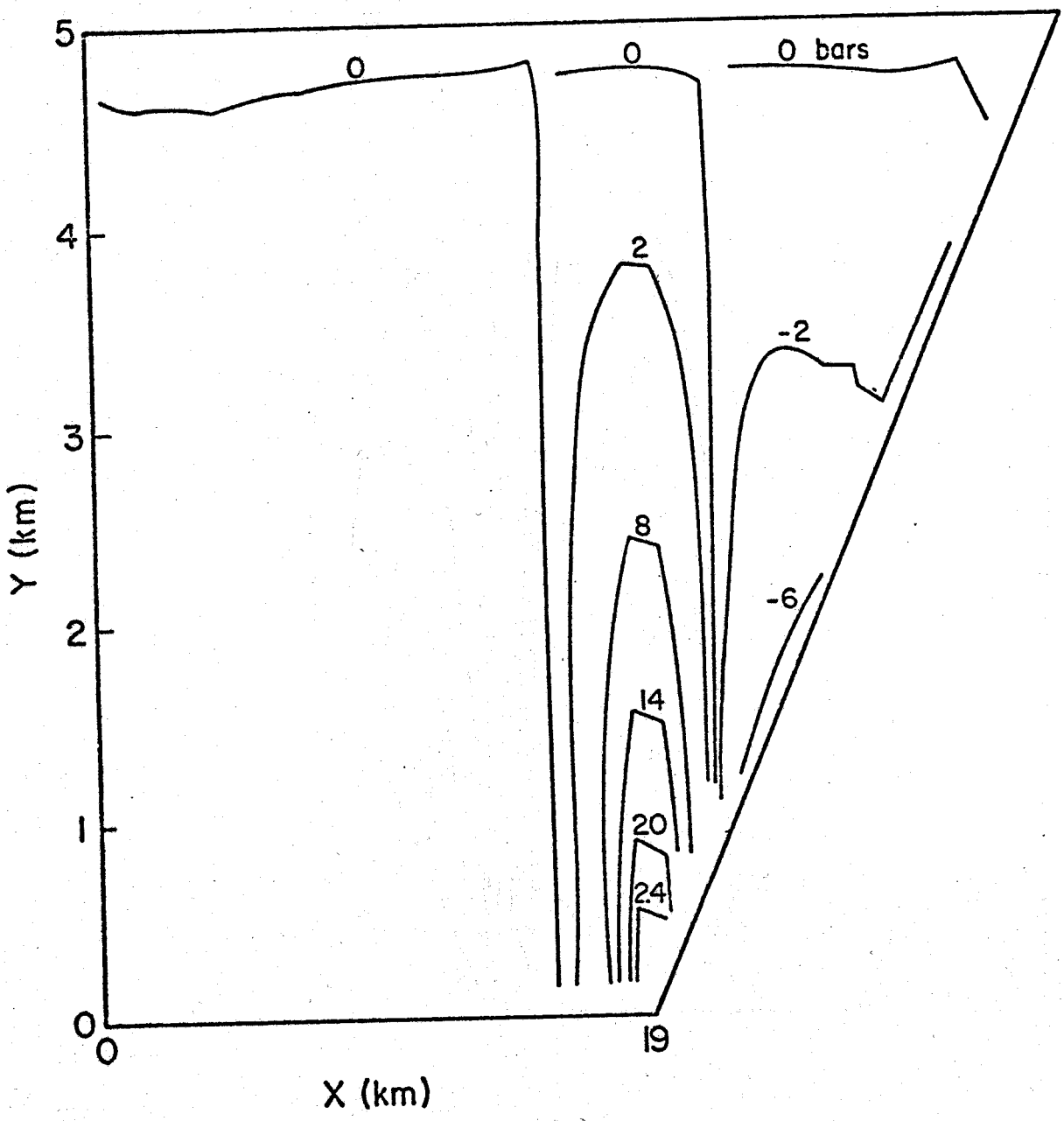

Figure 4.16. $\Delta\sigma_y$ [$=\sigma_y$ (t = 55.2 years) - σ_y (t = 0 years)] contours.

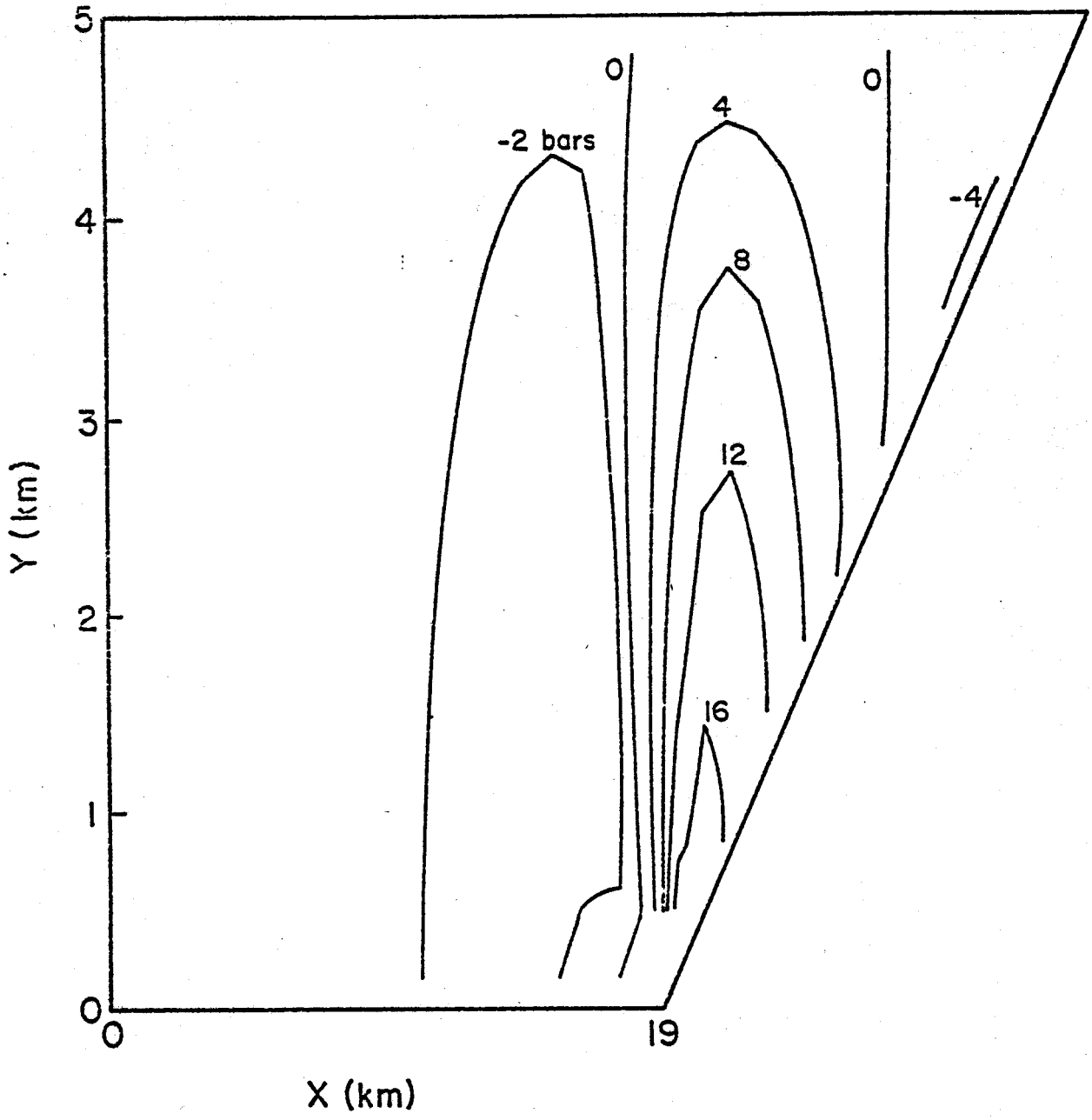

Figure 4.17. $\Delta\sigma_{xy}$ [$=\sigma_{xy}$ (t = 55.2 years) - σ_{xy} (t = 0 years)] contours.

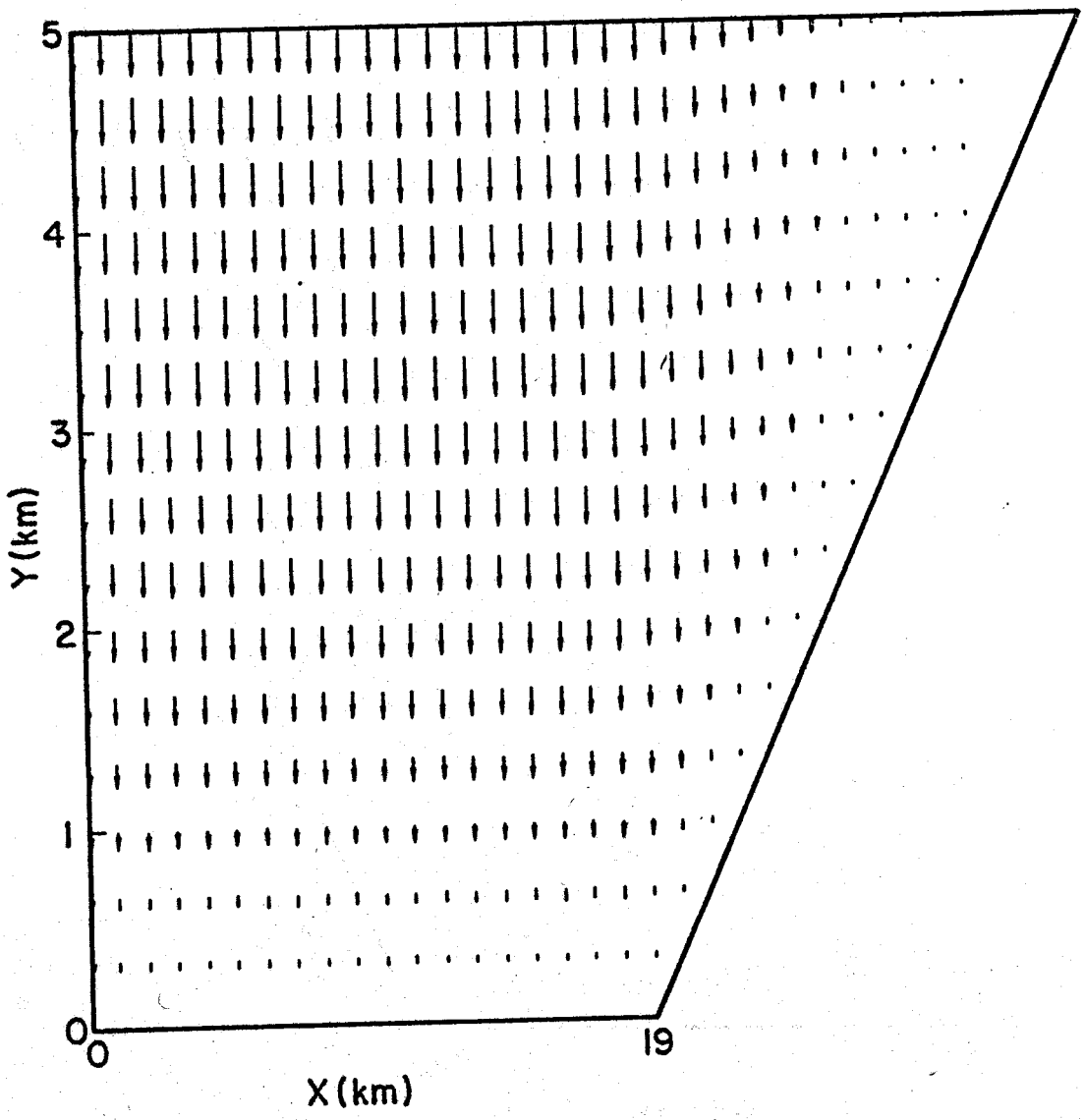

Figure 4.18. Displacement vectors at t = 55.2 years (vector maximum = 8.702 m).

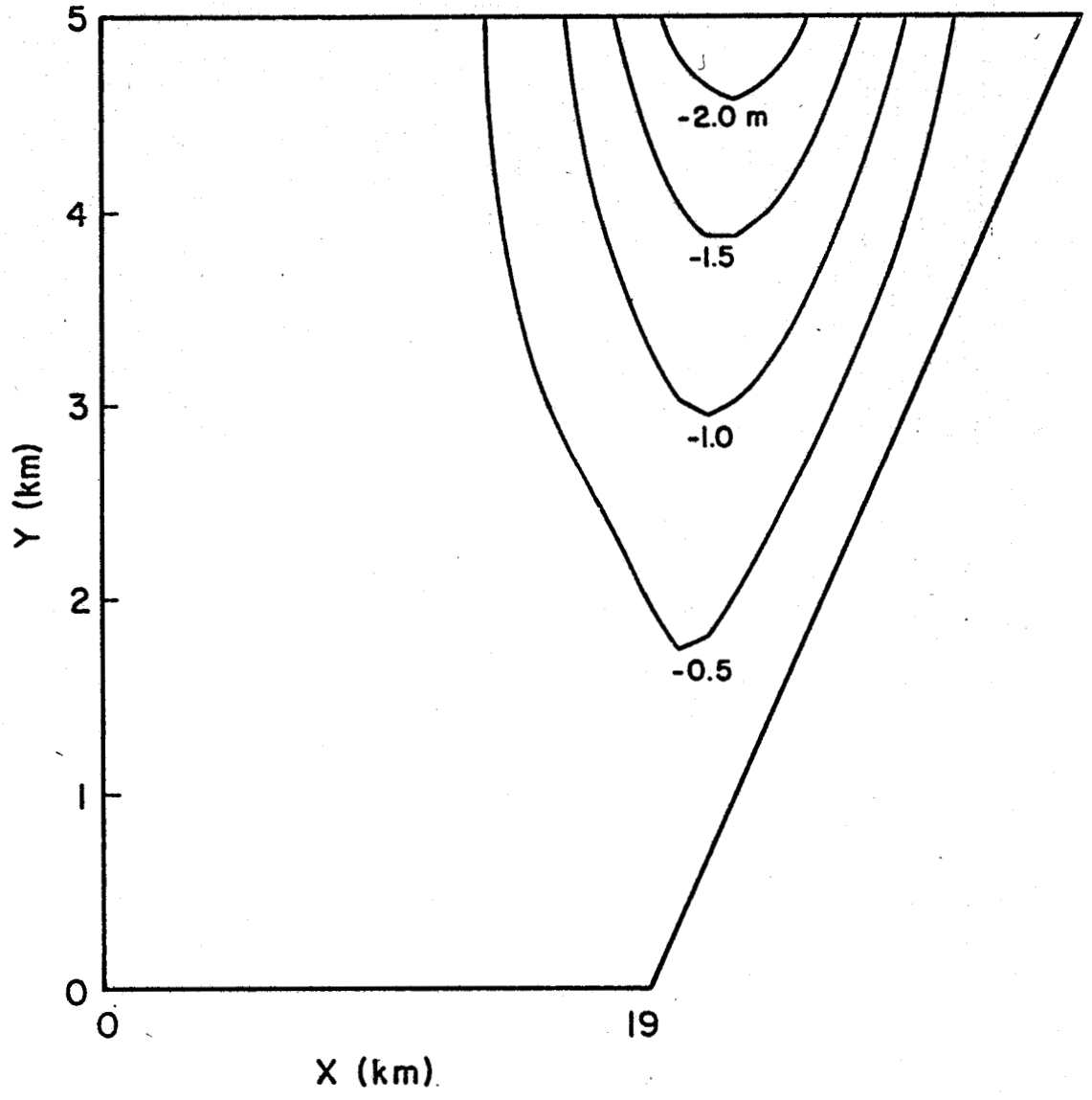

Figure 4.19. Horizontal displacement (= $u_{55.2} - u_0$) contours at t = 55.2 years.

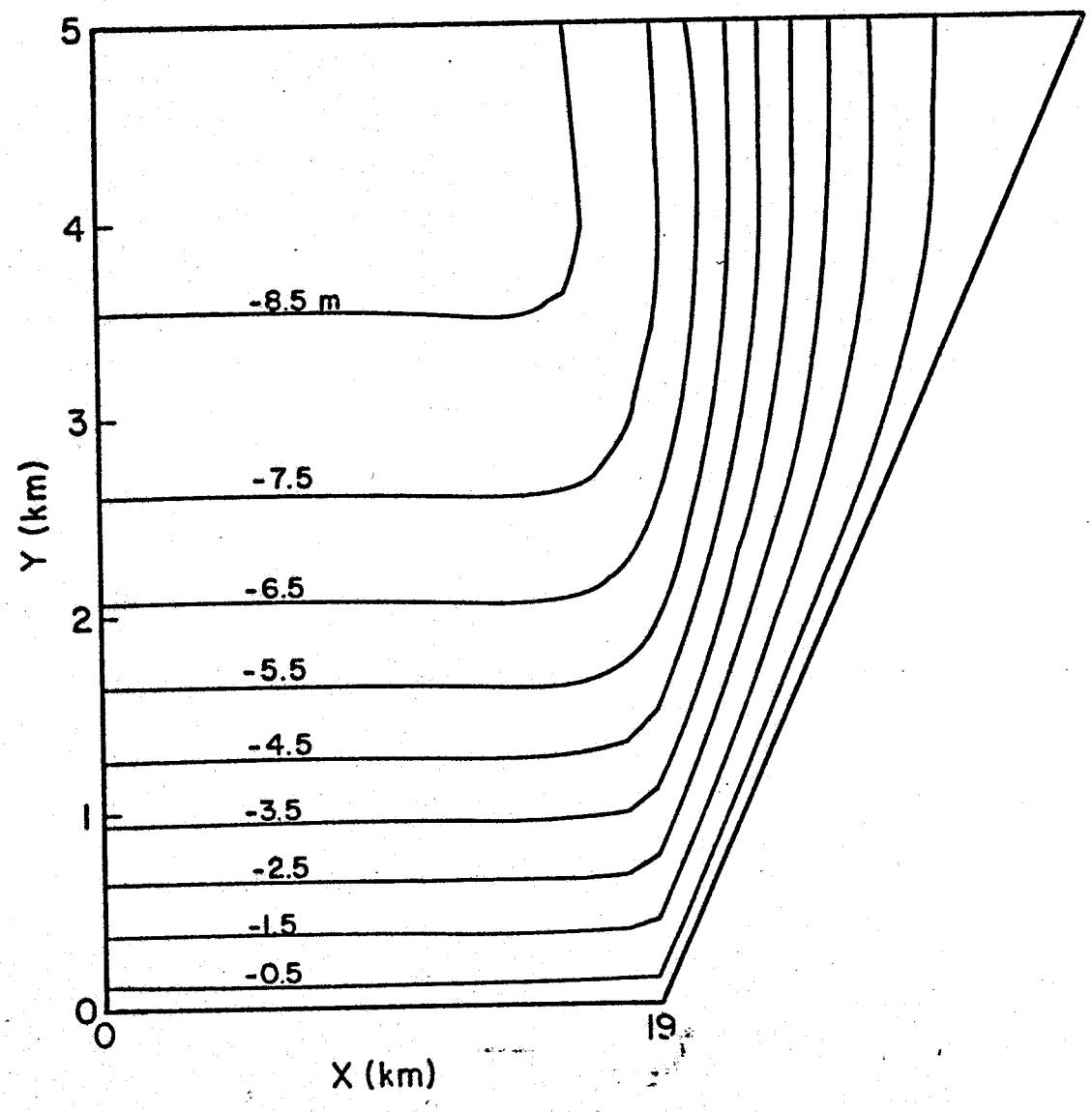

Figure 4.20. Vertical displacement (= $v_{55.2} - v_0$) contours at t = 55.2 years.

into account both horizontal and vertical motions of the ground surface.

The preliminary calculations presented in this section clearly show that fluid production without injection can lead to large surface deformations. To obtain a more realistic theoretical model, it would be necessary to utilize a coupled rock deformation-fluid diffusion model (Section III). Furthermore, application of the theoretical model to simulate real geothermal reservoirs will, of course, require taking into account realistic geometries and rock properties, pre-existing faults, and additional factors such as heterogeneous rock formations and fluid injection.

V. AUXILIARY PROBLEMS

The 3D coupled reservoir simulator, when completed in Phase II of this research effort, should be adequate to describe the response of the geothermal field as a whole. Production and injection wells can be represented within the three-dimensional mesh as point sources and sinks of fluid. Then the code will calculate the fluid and solid motions over the producing life of the field. Thus, for example, regions of subsidence or surface swelling may be predicted and production strategy adjusted to minimize the hazard. There are, however, a number of effects which must be treated separately. These effects are either of environmental consequence in themselves, or are needed to supplement and support the calculations of the 3D reservoir model. In this section, we discuss two of these, namely seismic hazards (Section 5.1) and geochemical effects (Section 5.2). Preliminary work was done in Phase I in each of these areas and only a very limited effort is possible within the scope of Phase II.

5.1 SEISMIC RISK

Fluid injection in the presence of large tectonic stresses can lead to shear failure and fault slippage. As examples, we cite the experience at Rocky Mountain Arsenal near Denver, Colorado (e.g., Healy, et al. [1968]), and Rangley field, Colorado (Rayleigh [1971], Healy [1971]). In both of these cases as the water was driven into the faulted region, small earthquakes began to occur. When the pumping was stopped, the occurrence of earthquakes persisted for a period, then as the fluid pressure declined by continued diffusion, the earthquake activity also diminished. Many geothermal reservoirs (including those in Imperial Valley and the Gulf Coast) lie in regions of extensive faulting;

thus the danger of earthquake triggering through subsurface injection of waste fluids cannot be discounted.

In order to make a good estimate of seismic risk in any given geothermal area, we must know (1) the state of tectonic stress, (2) the rate at which it is accumulating, (3) the mechanics of faulting, and in particular the role of fluid pressure and the relation between injection and induced earthquake magnitude, and (4) pore pressure and flow associated with the geothermal operation. Each one of these four items requires a model due to our limited knowledge in most practical situations.

An effort was initiated (in collaboration with Dr. Amos Nur of Stanford University) during Phase I to assemble the statistical seismic data for the Imperial Valley, available in the literature (Allen, et al. [1965]; Hileman, et al. [1973]) which may be related to items (1) and (2). The Salton Sea/Imperial Valley/Mexicali Valley geothermal basin is a sediment-filled rift valley which is, in effect, the northerly landward extension of the Gulf of California. The region is heavily faulted in a roughly NW-SE direction, being bounded on the southwest by the San Jacinto Fault and on the northeast by the San Andreas Fault. Several smaller faults also pass through the valley. The East Pacific Rise (a sea-floor spreading center) is believed to underlie both the Gulf of California and the geothermal rift zone, and is responsible for the abnormally high heat fluxes found throughout the area. The basement rock in most of the region is well over 4 kilometers below the present land surface. Several regions of potential interest for geothermal extraction have been identified, including the Cerro Prieto field in Mexico, the Dunes and Mesa anomalies, and the Buttes region on the southern shore of the Salton Sea. Figure 5.1 is a base map of the Southern California region with major faults; an enlarged view of the Salton Sea/Imperial Valley/Mexicali Valley

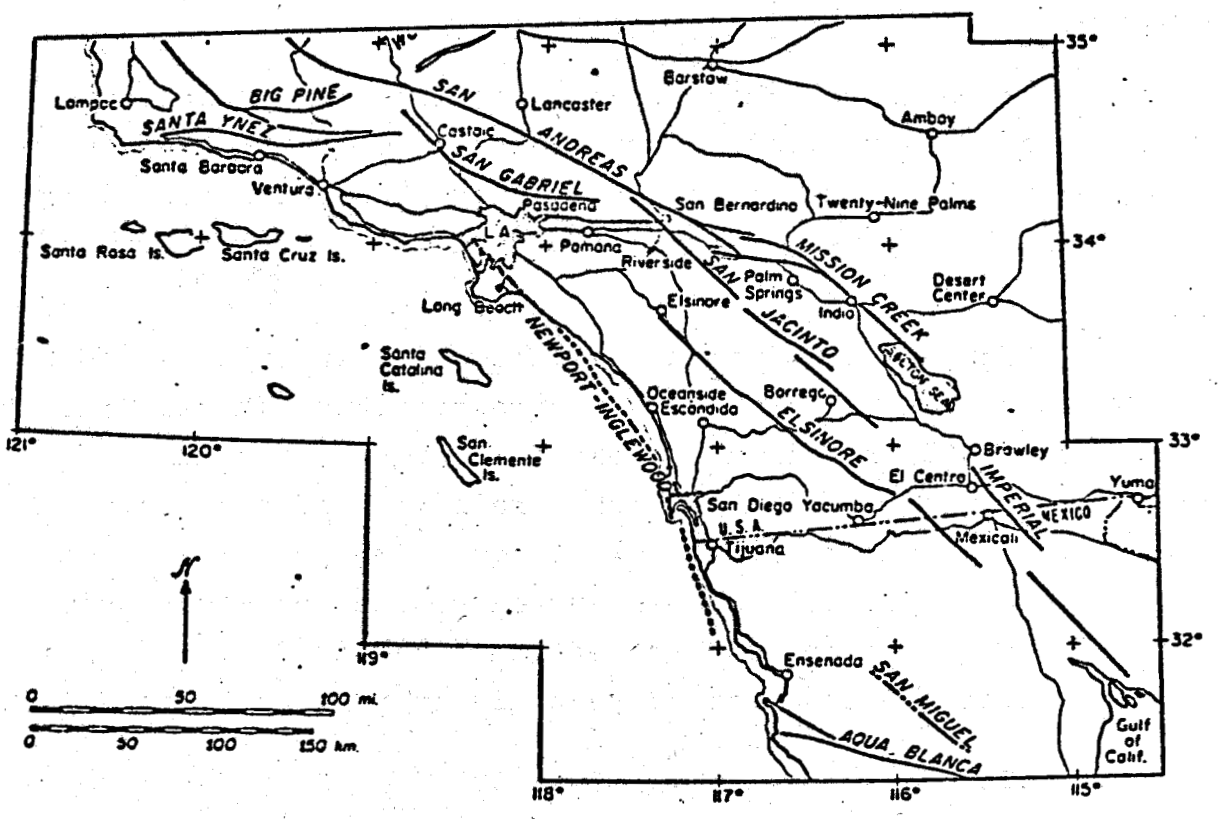

Figure 5.1. Base map of Southern California region with major faults (Hileman, et al. [1973]).

geothermal basin is shown in Fig. 5.2. Geothermal areas such as Buttes/Salton Sea and Mesa are seen to lie in seismically active regions (see Figs. 5.1 - 5.3). It is clear, from Fig. 5.3 that conclusions about future seismicity and the present state of stress in the small areas of the Buttes and Mesa are liable to be uncertain.

If we assume that local injection and pumping operations cause only local deformation and do not trigger earthquakes which are substantially larger than the affected injection volume, we can estimate the tectonic state from past seismicity.

Figure 5.3 shows the estimated strain release, in numbers of equivalent Richter scale magnitude (M = 3.0) earthquakes per 100 km^2 in the area of interest. Both the Buttes and Mesa areas are in the high strain release zone in which an expected number of N = 64-256 equivalent M = 3.0 earthquakes occur per 100 km^2 per 30 years. In terms of equivalent earthquakes per 100 km^2 of other magnitudes, the estimated strain release per 30 years is approximately as follows:

Magnitude	0	1	2	3	4	5	6
Equivalent	∿25,000	3600	600	100	16	2.5	0.4

If we take 10 km × 10 km as a typical area of a geothermal operation we can combine the total strain release with the observed frequency N and magnitude M relation, to estimate the liklihood of occurrence of earthquakes in the area:

$$\log N = a - bM$$

where a and b are constants. For M = 0, the number of events N over 30 years is approximately 10,000 - 50,000; per year we get 300 - 1500 events (of M = 0), and thus $a \approx 2 - 3$. As shown in Fig. 5.4, b = 0.85 for the Imperial Valley.

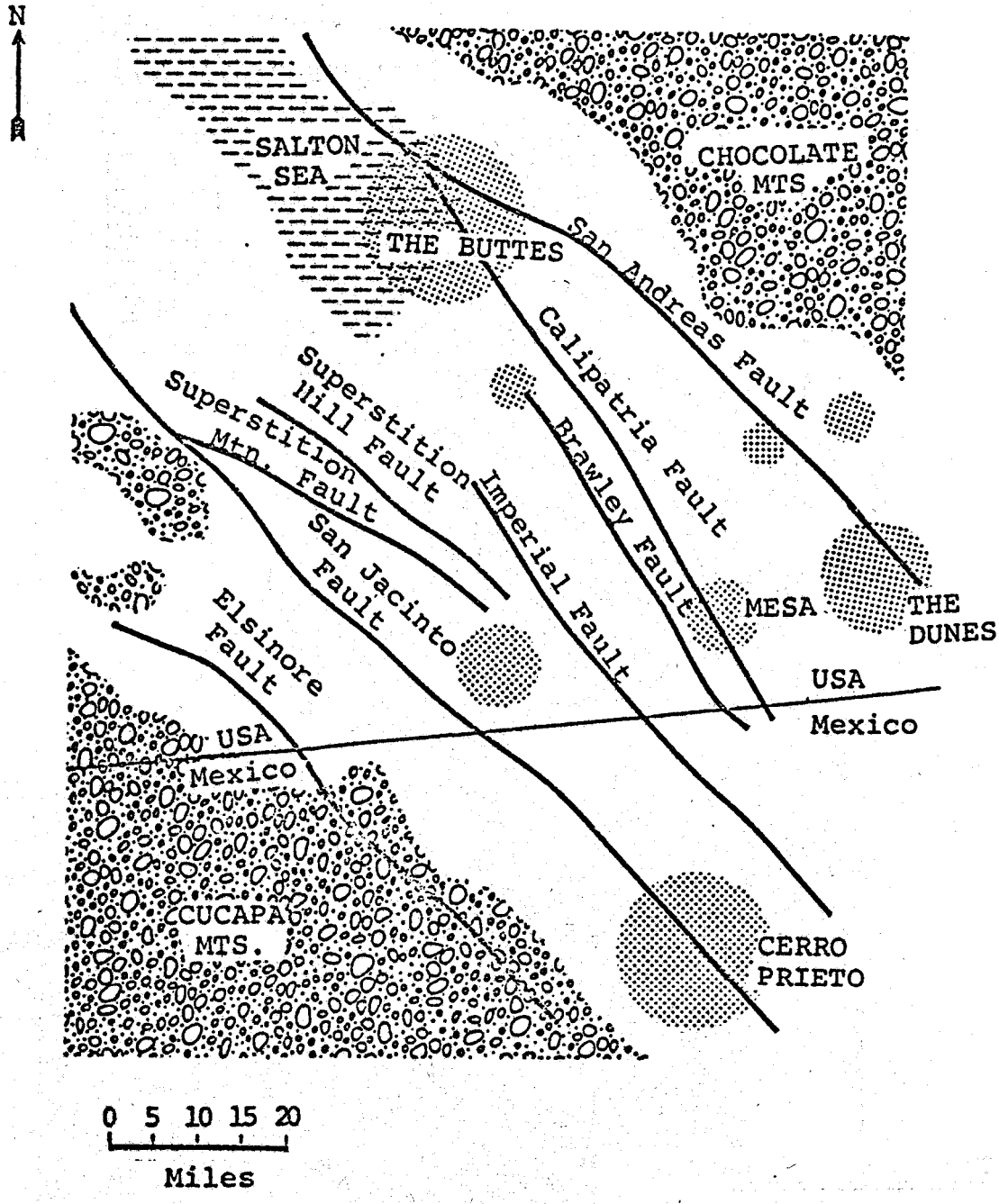

Figure 5.2. The Salton Sea/Imperial Valley/Mexicali Valley geothermal basin. Geothermal anomalies shown as dotted areas.

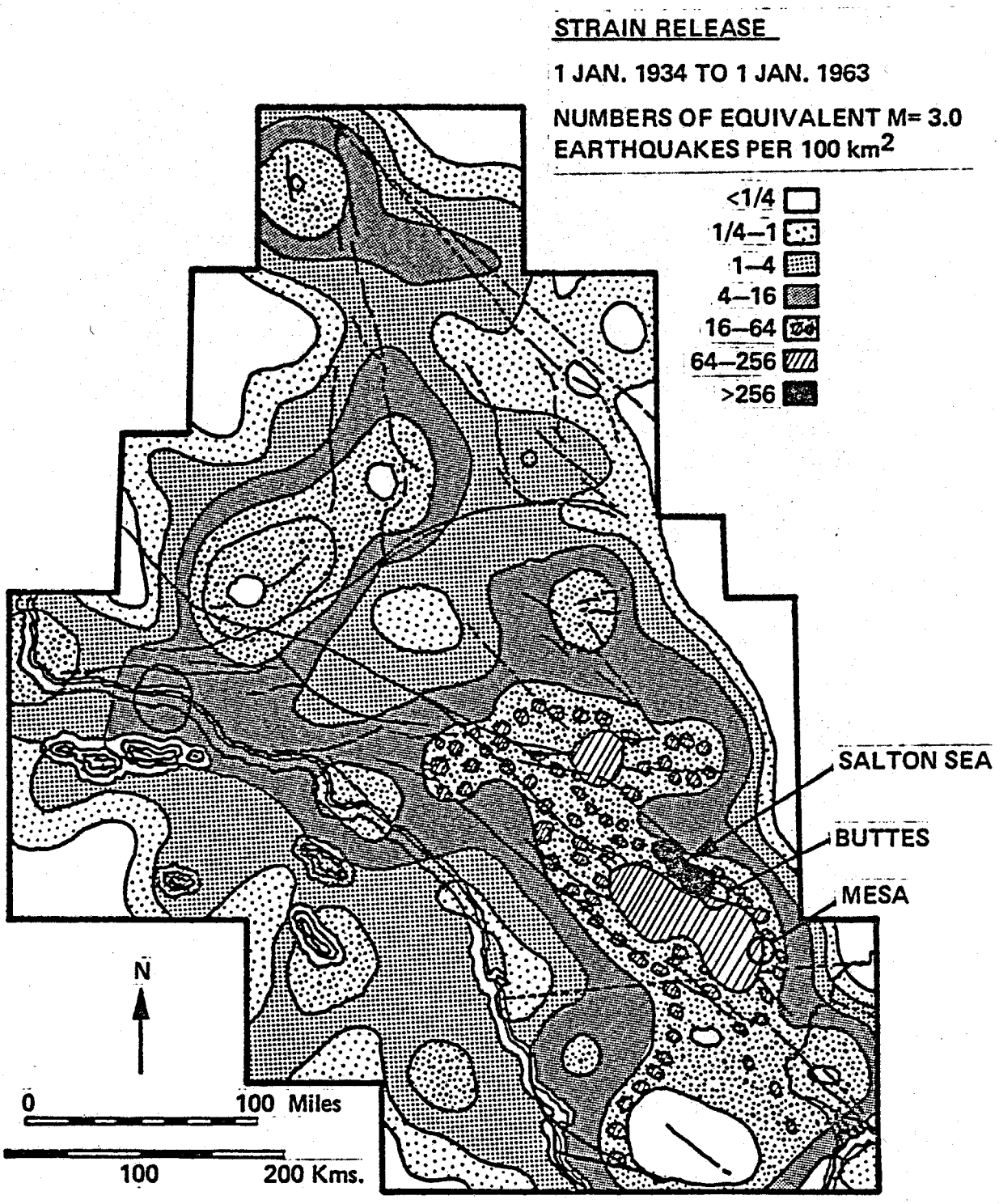

Figure 5.3. Smoothed strain-release map of Southern California region after ten iterations (Hileman, et al. [1973]).

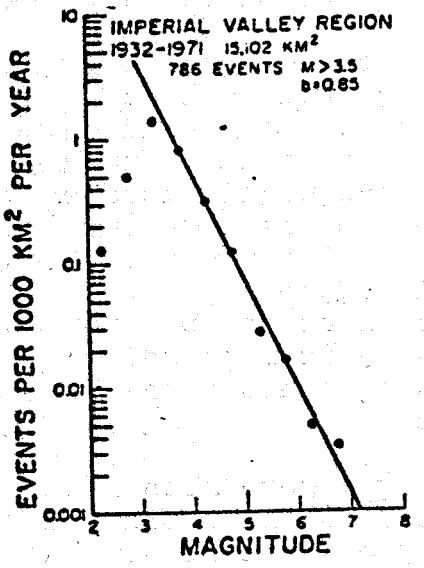

Figure 5.4. Number of events versus magnitude for Imperial Valley region (Hileman, et al. [1973]).

In other words, for undisturbed conditions we expect each year to have, in an 10 × 10 km^2 area, 300-1500 events of M = 0; 50 - 200 events of M = 1; 15 - 30 events of M = 2; 2 - 10 events of M = 3; 0.1 - 1 events of M = 4; and < 0.1 events of M = 5.

The question then is how will this natural seismicity be modified by injection and pumping, etc. To answer this we must make further assumptions. Two possibilities follow:

1. In the frequency-magnitude relation, log N = a - bM, assume that both a and b are physical parameters which depend on pore pressure. The parameter a is a measure of the overall seismic activity and would increase with injection. The parameter b is a measure of the number of large events relative to small events; preliminary results (laboratory and theory) exist which suggest that the value of b increases with pore pressure. Thus, there is more seismic activity and relatively more small events than large ones at high pore pressure.

2. We can try a more mechanical rather than statistical model, in which one actually computes the distribution of pore pressure and finds its effects on triggering of slippage on a hypothetical fault plane.

This information, along with other relevant data, will be utilized during Phase III (third year) of this program to evaluate limiting conditions under various production and reinjection strategies.

5.2 GEOCHEMICAL EFFECTS

Reinjection of geothermal fluids following power extraction may induce undesirable chemical effects in subsurface geological strata. For example, the brines may undergo chemical changes during the extraction process, particularly if they are temporarily stored above ground prior to reinjection. In such a case, opportunity for oxidation, e.g., conversion of Fe^{++} to Fe^{+++}, occurs. Upon reinjection, the brines would not be in chemical equilibrium with the rock strata at the reinjection site. Chemical reactions might then occur which would lead to the formation of undesirable species in the rock strata; for instance, the production of clay-like minerals which could penetrate the pores and render some strata impervious. Continued reinjection at the site would then become impossible. Because of the significance of such possibilities, a limited effort was made during Phase I to use a set of existing geochemical computer codes to analyze reinjection chemistry.

The first objective of this geochemical effort was to bring the PATH computer program developed by Dr. Harold Helgeson of the University of California at Berkeley on-line and operational at S^3. (Dr. Helgeson participated as a consultant to S^3.) The intention was to then utilize this program to carry out a set of calculations to simulate the behavior of Salton Sea brines during cooling. Such a calculation would have predicted possible chemical reactions between brine constituents, or precipitation or scaling reactions which might occur as a consequence of the temperature drop accompanying power extraction. Had this calculation been successful, we would then have considered chemical processes which might accompany reinjection of this cold brine into representative rock strata.

The above-planned calculation was not successfully achieved because of difficulties associated with the version of the PATH-1 code which S^3 had acquired at the beginning of the program. The nature of these difficulties will be briefly discussed here.

The Helgeson PATH-1 code was written for Control Data Corporations 6000-series computers and is adaptable to more advanced CDC computers. In principle, it should be applicable with ease to other (non-CDC) computers as well, but in practice it is not since it was written in a modified FORTRAN language utilizing a syntax for many instructions which is not interpretable by non-CDC compilers. No consideration is given in PATH-1 to the magnitude of the variables which enter the problem, so that upon transition to a computer whose range of scale is less than that of the CDC machines, problems of underflow and/or overflow frequently arise. Furthermore, PATH-1 does not utilize core storage efficiently; thus, a machine with a smaller core memory cannot be used without exceeding core capacity. This storage problem does not arise because of any inherent need for massive data storage in the geochemical problem. For instance, the PATH-1 program saves the elemental composition of 131 minerals and 122 solution species (approximately 20 elements being considered) all in core memory. Approximately 5,000 words are thus used, about 80 percent of which turn out to be zero. More efficient coding would obviate the need to enter 4,000 superfluous zeros into core.

As a consequence of these coding difficulties, a significant effort was needed to render the PATH-1 program functional on the S^3 Univac 1108 computer. The conversion steps included:

1. Revision of nontransferrable syntax.
2. Conversion of key unscaled variables from single to double precision.
3. Reallocation of core storage, and utilization of peripheral storage.

The third item was necessary as a direct consequence of the second: because of lack of scaling, higher precision was needed (this because the Univac word is 36 bits long, as against the CDC word's 60 bits). But higher precision increases storage demand, and the program was already core-limited.

By January, 1975 a new version (PATH-2) of Helgeson's code was generated which was apparently functional on the Univac 1108. A number of test runs on simplified problems were successfully carried out. In late January, 1975, initial efforts were made to use this program to solve a simple but meaningful geochemical problem. The objective was to determine a thermodynamically valid solution composition which might be found in equilibrium with a rock stratum characteristic of a Salton Sea brine source. We considered the reaction of a brine, initially composed of CaCl-KCl-$CaCl_2$ (with small amounts of $ZnCl_2$ also included), in contact at 300°C and saturation pressure, with a rock matrix composed of 25 mole precent microcline, 42 mole percent low albite, 9 mole percent anorthite, 12 mole percent annite, and 12 mole percent phlogopite.

PATH-2 was unable to solve this problem. Although composition changes could be followed for some time as the computation advanced, and both the appearance and disappearance of various phases could be observed, the program always broke down prior to completion. Apparently, the program is unreliable for a system of this complexity. It appears that the algorithms used in the program accumulate errors as the calculation advances, until finally some critical limitation

is exceeded which leads to a breakdown. Much computer time was thus spent in futile calculation. At the same time, it is important to realize that the chemical process described above is unique and completely defined, and that with a properly designed algorithm no breakdown should occur.

Early in 1975, we learned that Dr. Claude Herrick of Los Alamos Scientific Laboratory had also received a copy of PATH-1 from Dr. Helgeson and had corrected several of the original programming deficiencies. Dr. Herrick kindly supplied us with a tape listing of his program PTCALC, and his data base (the data base was nearly identical to the one we had already been using). The decision was made to abandon Helgeson's program and instead use Herrick's program. This decision, which we believe to be the correct one, put us back where we were at the start of Phase I, because Herrick's program, like Helgeson's, was written for the CDC series computers, and was incompatible with our Univac system in syntax, precision, and storage requirements. Nevertheless, we once more undertook the modifications, and at the end of Phase I have completed the syntax conversion, which we believe to be roughly 50 percent of the conversion job. Upon completion of the conversion, we could recommence the geochemical calculations we had intended to perform earlier.

At the same time, we anticipate that Herrick's program also may not be entirely suitable. Dr. Herrick has indicated to us that a calculation of the chemical reaction of a brine with an eight phase rock matrix, which is the most complex calculation he has been able to handle, requires between one-half and two hours on the CDC 7600. Translated to the Univac 1108, with the requisite upgrading in precision, core structure, and syntax, computing time for a comparable problem should range between four and eight hours. We believe that such computing times are excessive for a problem of this character; if four hours are required for this <u>one</u> calculation,

many times four hours will be required for a thorough study of possible geochemical processes in the Salton Sea.

We believe, however, that there is a preferable alternative. Analysis of the Herrick and Helgeson programs suggests that a more efficient numerical algorithm and more careful programming could reduce computing time and costs by one to two orders of magnitude. For example, the program recently developed by Morel and Morgan [1972] handles large systems much more effectively than the Helgeson-Herrick scheme. Unfortunately, the Morel-Morgan program is not directly applicable to multiphase geothermal systems, because it functions only at constant (and not variable) ionic strength. Nevertheless, the fact that their program computes multi-component solution equilibrium in seconds instead of minutes is a clear indication of the possibilities for improvement.

Furthermore, computer programs which deal with equilibria in nonideal gas-solid systems have been available for many years, and are accurate, reliable, and very fast. We believe that the concepts used in these gas-solid programs should be adaptable to liquid systems. If we were free to pursue the path leading to the greatest long-term benefits, we would elect to develop an entirely new program to replace both the available programs, but such an effort is outside the scope of the present grant. Therefore, no work in geochemistry is contemplated in Phase II of this program; a separate project to develop an improved geochemistry computer program will be proposed.

VI. CURRENT WORK PLAN

The ability to treat mechanical rock-fluid interactions is essential for evaluating certain geohydrological environmental effects such as subsidence and seismic hazards (Section I). Work is presently proceeding (under Phase II of this program) on coupling the quasi-active fluid flow model (Section 3.1) to the rock response model (Section 3.2). The coupling procedure was briefly described in Section 3.3. It is anticipated that the coupled three-dimensional reservoir simulator will be fully operational within the next two to three months. Emphasis will then shift towards making calculations to validate and apply the computer model using geothermal field production data.

The four major geothermal fields presently in operation are the Geysers field in the United States, the Larderello field in Italy, the Cerro Prieto field in Mexico, and the Wairakei field in New Zealand. We have chosen to analyze the Wairakei field in the upcoming year for two main reasons. First of all, it is an established power producing area with a significant amount of available data dating from 1953 (see, e.g., Grindley [1965]; Bolton [1968, 1970, 1973, 1975]). Secondly, it is a hot water-dominated reservoir similar in this aspect to the Salton Sea geothermal field, our ultimate research objective.

During Phase II, we are attempting to match both the gross reservoir performance and subsidence measurements for the Wairakei field. Considerable amount of production and subsidence data have already been obtained from the New Zealand researchers. The New Zealand Ministry of Works (MOW) and Department of Scientific and Industrial Research (DSIR) have also made available to us core samples of the reservoir rock. As part of the modeling effort for Wairakei, Terra Tek, Inc. acting as subcontractor to S^3, is currently conducting laboratory tests to establish the rock properties required in the

reservoir simulation model described in Sections II and III. Arrangements are also being made under the S^3/MOW cooperative effort to obtain *in situ* seismic velocities for the Wairakei formations.

Imperial Valley geothermal fluids, unlike those in Wairakei, contain substantial amounts of dissolved salts. For example, the geothermal fluids in the Salton Sea field contain more than 25 percent by weight dissolved solids (that is, about ten times more saline than sea water). The dissolved salts can significantly alter the thermo-physical properties of water. We, therefore, plan to develop a computerized equation of state describing the thermophysical properties of brines for the salinity, temperature, and pressure domain of interest. Data for these composition and pressure-temperature domains will be sought from the literature and from contacts with other researchers (e.g., University of California at Berkeley, Los Alamos Scientific Laboratory, New Zealand Department of Scientific and Industrial Research, and the U.S. Geological Survey) to provide information on phase changes, heat capacities, viscosities, enthalpies and other variables.

The hot concentrated brines characteristic of Imperial Valley fields can cause serious corrosion and scaling problems in the turbines, well casings, any downhole apparatus, transmission piping, separators, and so on. Additionally, there exists the danger of polluting fresh ground waters (Section I). *In situ* flashing has been suggested as one means of overcoming these problems. Presumably, the solids have limited solubility in steam and would be deposited in the formation. During the current phase of the program (Phase II), we plan to investigate the production strategies required for in-formation flashing; particular attention will be paid to the effects of precipitated solids on near-wellbore permeability.

Successful completion of the work outlined in the above paragraphs will materially enhance our ability to perform predictive calculations for the Salton Sea geothermal field. At this time, we anticipate making these calculations sometime during the early part of the third year of this program (Phase III).

REFERENCES

Allen, C. R., P. St. Amand, C. F. Richter, and J. M. Nordquist, "Relationship Between Seismicity and Geologic Structure in the Southern California Region," Bulletin Seismological Society of America, Vol. 55, p. 753, 1965.

Arihara, N., "A Study of Non-Isothermal Single and Two-Phase Flow Through Consolidated Sandstones," Stanford Geothermal Program Report SGP-TR-2, 1974.

Bolton, R. S., "Analysis of Downhole Pressure Measurements Taken During the Partial Shutdown — December 12, 1967 to April 4, 1968," New Zealand Ministry of Works Report, 1968.

Bolton, R. S.,"The Behavior of the Wairakei Geothermal Field During Exploitation," U.N. Symposium on the Development and Utilization of Geothermal Resources, Pisa, 1970.

Bolton, R. S., "Management of a Geothermal Field," Geothermal Energy (Earth Sciences 12), UNESCO, 1973.

Bolton, R. S., personal communication (miscellaneous microfilm, tabular and magnetic tape data), 1975.

Bories, S. A., and M. A. Combarnous, "Natural Convection in a Sloping Porous Layer," Journal of Fluid Mechanics, Vol. 57, p. 63, 1973.

Brace, W. F., "Pore Pressure in Geophysics," Flow and Fracture of Rocks, American Geophysical Union, Washington, D. C., p. 265, 1972.

Brownell, D. H., Jr., S. K. Garg, and J. W. Pritchett, "Computer Simulation of Geothermal Reservoirs," Society of Petroleum Engineers, Paper No. SPE 5381, 1975.

Budiansky, B., "Thermal and Thermoelastic Properties of Isotropic Composites," Journal of Composite Materials, Vol. 4, p. 286, 1970.

Corey, A. T., C. H. Rathjens, J. H. Henderson, and R. J. Wyllie, "Three-Phase Relative Permeability," Transactions AIME, Vol. 207, p. 349, 1956.

Desai, C. S., and J. F. Abel, "Introduction to the Finite Element Method," New York, Chapter 7, 1972.

Dahlquist, G., and Ake Bjorck, "Numerical Methods," Englewood Cliff, New Jersey, Section 5.3, 1974.

Donaldson, I. G., "Temperature Gradients in the Upper Layers of the Earth's Crust due to Convective Water Flows," Journal of Geophysical Research, Vol. 67, p. 3449, 1962.

Donaldson, I. G., "The Flow of Steam Water Mixtures Through Permeable Beds: A Simple Simulation of a Natural Undisturbed Hydrothermal Region," New Zealand Journal of Science, Vol. 11, p. 3, 1968.

Elder, J. W., "Steady Free Convection in a Porous Medium Heated from Below," Journal of Fluid Mechanics, Vol. 27, p. 29, 1974a.

Elder, J. W., "Transient Convection in a Porous Medium," Journal of Fluid Mechanics, Vol. 27, p. 609, 1967b.

Garg, S. K., "Wave Propagation Effects in a Fluid-Saturated Porous Solid," Journal of Geophysical Research, Vol. 76, p. 7947, 1971.

Garg, S. K., and A. Nur, "Effective Stress Laws for Fluid-Saturated Porous Rocks," Journal of Geophysical Research, Vol. 78, p. 5911, 1973.

Garg, S. K., D. H. Brownell, Jr., J. W. Pritchett, and R. G. Herrmann, "Shock Wave Propagation in Fluid-Saturated Porous Media," Journal of Applied Physics, Vol. 46, p. 702, 1975a.

Garg, S. K., J. W. Pritchett, and D. H. Brownell, Jr., "Transport of Mass and Energy in Porous Media," to appear in the Proceedings of the Second United Nations Symposium on the Development and Use of Geothermal Resources, San Francisco, California, May 19-29, 1975b.

Garg, S. K., J. W. Pritchett, D. H. Brownell, Jr., and J. Sweet, "Multiphase Fluid-Flow in Geologic Media and Land Surface Subsidence," Proceedings, Society of Engineering Science Meeting, Austin, Texas, October 20-22, 1975c.

Grindley, G. W., "The Geology Structure, Exploitation of the Wairakei Field, Taupo, New Zealand," New Zealand Geological Survey Bulletin No. 75, 1965.

Healy, J. H., W. W. Rubey, D. T. Griggs, and C. B. Rayleigh, "The Denver Earthquakes," Science, Vol. 161, p. 1301, 1968.

Healy, J. H., "Rangely Microearthquakes," presentation at the Penrose Conference, Snowmass at Aspen, Colorado, September 1971.

Hileman, J. A., C. R. Allen, and J. M. Nordquist, "Seismicity of Southern California Region," Report Seismological Laboratory, California Institute of Technology, Pasadena, California, 1973.

Kruger, P., and H. Ramey, Jr., "Stimulation and Reservoir Engineering of Geothermal Resources," Stanford Geothermal Program Report SGP-TR-1, 1974.

Mercer, J. W., Jr., C. Faust, and G. F. Pinder, "Geothermal Reservoir Simulation," Proceedings of NSF/RANN Conference on Research for the Development of Geothermal Energy Resources, p. 256, Jet Propulsion Laboratory/California Institute of Technology, Pasadena, California, 1974.

Morel, F., and J. Morgan, "Numerical Method for Computing Equilibria in Aqueous Chemical Systems," Environmental Science and Technology, Vol. 6, p. 58, 1972.

Morland, L. W., "A Simple Constitutive Theory for a Fluid-Saturated Porous Solid," Journal of Geophysical Research, Vol. 77, p. 890, 1972.

Nayfeh, A. H., D. H. Brownell, Jr., and S. K. Garg, "Heat Exchange in a Fluid Percolating Through Porous Media," Proceedings Society of Engineering Science Meeting, Austin, Texas, October 20-22, 1975.

Ramey, H. J., Jr., W. E. Brigham, H. K. Chen, P. G. Atkinson and N. Arihara, "Thermodynamic and Hydrodynamic Properties of Hydorthermal Systems," Stanford Geothermal Program Report, SGP-TR-6, April 1974.

Rayleigh, C. B., "Rangely, Colorado," presentation at the Penrose Conference, Snowmass at Aspen, Colorado, September 1971.

Scheidegger, A. E., "Hydrodynamics in Porous Media," Handbuch der Physik, Vol. VIII/2, Springer-Verlag, Berlin, p. 625, 1963.

Wooding, R. A., "Steady State Free Thermal Convection of Liquid in a Saturated Permeable Medium," Journal of Fluid Mechanics, Vol. 2, p. 273, 1957.

Wooding, R. A., "Convection in a Saturated Porous Medium at Large Rayleigh or Peclet Number," Journal of Fluid Mechanics, Vol. 15, p. 527, 1963.